Article

Identification of 4-Phenoxyquinoline Based Inhibitors for L1196M Mutant of Anaplastic Lymphoma Kinase by Structure-Based Design

shinmee mah, Jung Hee Park, Hoi-Yun Jung, Kukcheol Ahn, Soyeon Choi, Hyun Seop Tae, Kyung Hee Jung, Jin Kyung Rho, Jae Cheol Lee, Soon-Sun Hong, and Sungwoo Hong

Just Accepted

Identification of 4-Phenoxyquinoline Based Inhibitors for L1196M Mutant of Anaplastic Lymphoma Kinase by Structure-Based Design

Shinmee Mah,[a,b+] Jung Hee Park,[c+] Hoi-Yun Jung,[a,b] Kukcheol Ahn,[a,b] Soyeon Choi,[a,b] Hyun Seop Tae,[b] Kyung Hee Jung,[c] Jin Kyung Rho,[d] Jae Cheol Lee,[d] Soon-Sun Hong*[c] and Sungwoo Hong*[b,a]

[a]Department of Chemistry, Korea Advanced Institute of Science and Technology (KAIST), Daejeon 34141, Korea,

[b]Center for Catalytic Hydrocarbon Functionalizations, Institute of Basic Science (IBS), Daejeon 34141, Korea,

[c]Department of Biomedical Sciences, College of Medicine, Inha University, Incheon, 22212, Korea.

[d]Department of Asan Institute for Life Sciences and Oncology, Asan Medical Center, University of Ulsan, College of Medicine, Seoul 05505, Korea

RECEIVED DATE (to be automatically inserted after your manuscript is accepted if required according to the journal that you are submitting your paper to)

ABSTRACT

Dysregulation of anaplastic lymphoma kinase (ALK) has been detected in non-small cell lung cancer (NSCLC) in the form of EML4-ALK fusion. Secondary mutations opposing activity of the first generation ALK inhibitor crizotinib came into existence, requiring mutation-targeting drug discovery for the powerful second-line treatment. In this study, we report 4-phenoxyquinoline-based inhibitors that overcome crizotinib resistance to ALK L1196M, discovered by the fragment-growing strategy. The protonation of 4-aminoquinoline core could interrupt the ability the N atom of quinoline to act as a hydrogen bond acceptor; therefore, the pKa and calculated ionization pH values of relevant pyridine-based core moieties were carefully analyzed. The replacement of amine linkage with ether resulted in single-digit nanomolar range inhibitors. The inhibitors exhibited significant antiproliferative effects on H2228 CR crizotinib-resistant cells by decreasing PI3K/AKT and MAPK signaling. This work constitutes the first example for systematic investigation of the effect of ionization pH on activity in this system.

INTRODUCTION

Anaplastic lymphoma kinase (ALK) is a member of the receptor tyrosine kinases (RTKs) and the insulin receptor superfamily, and it is activated through dimerization upon binding the growth factor midkine (MK) and pleiotrophin (PTN) in the extracellular region. Activated ALK phosphorylates intracellular substrates and thereby switches on downstream cell signaling pathways to facilitate cell proliferation and survival signaling through the PI3K/AKT, JAK/STAT3 and MEK/ERK pathways.[1,2] Dysregulation of ALK signaling has been implicated in various human cancers, including non-small cell lung cancer (NSCLC), inflammatory myofibroblastic tumor, anaplastic large cell lymphoma, squamous cell carcinoma, and diffuse large B-cell lymphoma.[3-7] Therefore, the hyperactivation of ALK kinase has become a well-validated target for the development of therapeutics to treat several cancers. In addition, it has been demonstrated that the impairment of ALK activity with small-molecule inhibitors is effective in suppressing the growth of cancer in xenograft models in vivo.[8-11]

Accordingly, much effort has been devoted to the discovery of small-molecule ALK inhibitors, including crizotinib (Chart 1), the dual inhibitor of ALK and c-MET.[9,10, 12, 13] Despite the clear benefits of crizotinib, many ALK-dependent cancer cells tend to acquire various mutations that can render the ALK enzyme constitutively active by impeding the inhibitor binding in the ATP-binding site.[8, 14-20] The emergence of drug resistance has prevented the first-generation anti-NSCLC drug crizotinib from continued use in clinical treatment, which led to the development of the drug-resistant mutants of ALK. In particular, the mutation L1196M is most frequently identified in crizotinib-resistant patients. The emergence of the L1196M mutant has complicated clinical treatment, highlighting the importance of identifying new ALK inhibitors with high potency against the L1196M mutant. The substitution of Met for Leu could block the access of inhibitors to the deeper pocket near the gatekeeper residue in the ATP-binding site due to an increase in steric hindrance, representing a major obstacle for drug design.[22,23] In this regard, the identification of potent inhibitors that target the L1196M mutation would have important therapeutic implications.

The accumulation of three dimensional structure data on ALK-inhibitor interactions for various mutants has provided insight into overriding the drug resistance of ALK-dependent cancers.[24-27] Recently, we have revealed new molecular scaffolds for the development of new inhibitors targeting the L1196M mutant by the virtual screening of a large chemical library.[28] Our research was stimulated by the possibility that new inhibitors of the L1196M mutant could be rationally designed utilizing 3D structural information. This study was undertaken to identify new 4-quinoline-based inhibitors of the L1196M mutant of ALK through structure-based design strategies and to demonstrate the biological evaluation of various quinolone derivatives in terms of their anti-cancer effects on H2228 CR cells, which are crizotinib-resistant cells. A design strategy for improving their potency using electrostatic features and the effect of ionization pH of 4-quinoline scaffold to analyze the binding mode in detail was also discussed.

Chart 1. Chemical structures of crizotinib and representative 4-phenoxyquinoline based inhibitor.

Crizotinib

24, R = CH$_3$
30, R = OH
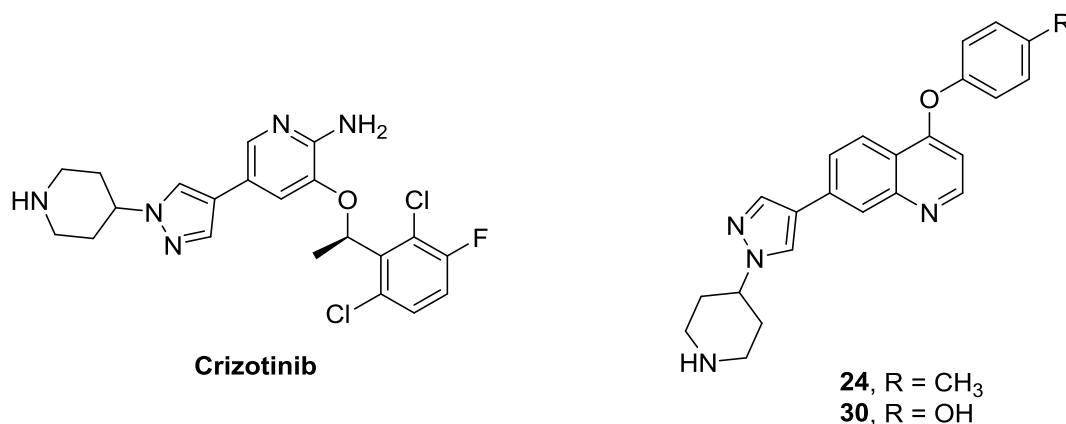
RESULTS AND DISCUSSION

Identification of 4-Aminoquinoline Moiety. With the goal of developing a new structural class of potent L1196M mutant inhibitors, we investigated the starting structure for *de novo* design and the affinity of various hinge-binding scaffolds to accommodate the increased bulk of the side chain of Met1196 in the ATP binding site, employing an L1196M crystal structure (PDB ID: 2YFX) as a template. Figure 1a shows the lowest energy conformation as calculated with the Discovery Studio 4.5 software. Based on comparing structural features and the interactions formed between various fragments and the L1196M mutant, the 4-aminoquinoline core appeared to be stabilized through hydrogen bonding with the backbone amide groups of a residue in the hinge region (Met1196) of the ATP-binding site. Interestingly, a larger gatekeeper Met1196 residue was found at the interface formed by van der Waals contacts between 4-aminoquinoline and the L1196M mutant (Figure 1b), indicating that favorable hydrophobic interactions were formed in the L1196M mutant. The quinoline serves as a hydrogen-bond acceptor with the backbone amidic nitrogen of Met1199 in the middle of the hinge region, whereas the 6-membered bicyclic aromatic ring of quinoline seems to be further stabilized through the van der Waals contacts of its aromatic rings with the side chains of Leu1122, Ala1148 and Leu1256. It is noteworthy that in the L1196M mutant, the increased steric hindrance of the gatekeeper mutation needs to be most carefully considered for drug design, and the 4-aminoquinoline scaffold resides in proximity to the side chain of the Met1196 gatekeeper without causing a steric clash. Because the 4-aminoquinoline scaffold binds tightly at the hinge
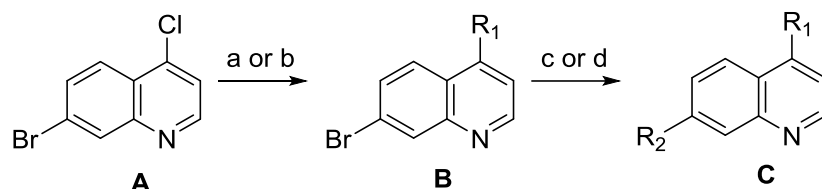
region (Met1199), it is predicted to serve as a good starting point from which potent inhibitors can be

derived. In addition, the 4-aminoquinoline scaffold can be easily diversified via a convergent synthetic

approach for the rapid elucidation of structure-activity relationship (SAR). The terminal 4-amino group

points toward the DFG (Asp1270-Phe1271-Gly1272) motif in the activation loop (A-loop) and a vacant

binding pocket comprising Arg1253-Asn1254-Cys1255-Leu1256-Gly1269-Asp1270 and Asp1203 to

accommodate a suitable fragment.[25] A significant improvement in potency is thus expected to result from

introducing a suitable chemical moiety at the terminal amino group. Furthermore, the ATP pocket is

connected to a narrow aisle composed of Glu1132, Leu1198 and Ala1200, implying that a fragment on

C7 of quinoline would be stabilized through hydrophobic interactions with the region near the solvent

front. Therefore, we planned to extend the structures by introducing various chemical moieties at these

two positions (Frag1 and Frag 2 in Figure 1b). For these reasons, 4-aminoquinoline was selected as a

putative core from which more potent inhibitors could be derived in our studies.
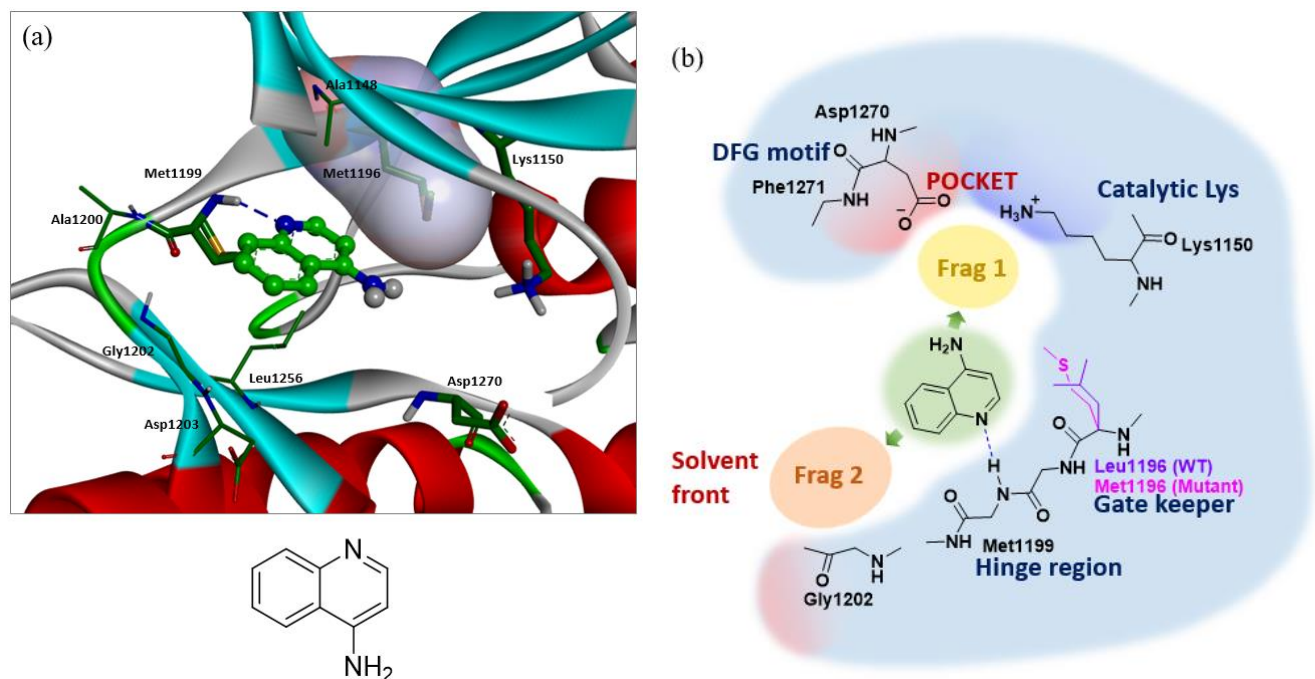
Figure 1. (a) Expected configuration of 4-aminoquinoline moiety in ATP binding site of ALK L1196M.

(b) Design of new scaffolds and opportunities for modification in the schematic active site of ALK

L1196M. Each dotted line represents a hydrogen bond.

   Chemical Synthesis. The *de novo* design process identified a variety of promising (hetero)arene

systems for introduction at the 4- and 7- positions of the quinoline core. The compound library was

established by a convenient route allowing the rapid exploration of the SAR profile and the general

synthetic route for representative quinolone derivatives, as shown in Scheme 1. The C4 position of

quinoline was functionalized with NH- or O-linked aryl groups prior to performing a Suzuki coupling

with the C7 (hetero)arene partners. The quinoline moiety can be easily equipped with a variety of

substituted anilines via addition and elimination processes under acidic conditions to afford the key

intermediate **B**.[29] An assortment of the C7 groups of 4-aminoquinolines were then explored through

palladium-catalyzed Suzuki cross-coupling with corresponding arylboronic acids or esters, affording the

desired product **C**. For a focused 4-phenoxy group array, S_NAr reactions between 7-bromo-4-

chloroquinoline and substituted phenol were conducted under basic conditions.[30] A variety of aryl groups

were then installed at the 7-position by Pd-catalyzed cross-coupling with the appropriate aryl boronic

acids or esters. An additional deprotection step removing the Boc-protection group of the solubilizing tail

was conducted to produce the final compounds.

Scheme 1. Synthesis of Quinoline Derivatives

A (Cl, Br, quinoline) → a or b → B (R_1, Br, quinoline) → c or d → C (R_1, R_2, quinoline)

3, R_2 = Ph
4, R_2 = pyridin-4-yl
5, R_2 = (2-aminopyridin-5-yl, H_2N)

6, R_2 = furan-2-yl
7, R_2 = thien-2-yl
8, R_2 = 1H-pyrazol-4-yl
9, R_2 = (1-methyl-1H-pyrazol-4-yl)

10, R_2 = (1-ethyl-1H-pyrazol-5-yl)

11, 14-30, R_2 = (1-(piperidin-4-yl)-1H-pyrazol-4-yl, HN)

12, R_2 = (1-(tetrahydro-2H-pyran-4-yl)-1H-pyrazol-4-yl, O)

2-12, R_1 = NHPh
14, R_1 = OPh
15, R_1 = NH-(2-F-Ph)
16, R_1 = O-(2-F-Ph)
17, R_1 = NH-(3-F-Ph)
18, R_1 = O-(3-F-Ph)
19, R_1 = NH-(4-F-Ph)
20, R_1 = O-(4-F-Ph)
21, R_1 = NH_2(3,4-diF-Ph)
22, R_1 = O-(3,4-diF-Ph)
23, R_1 = NH-(4-Me-Ph)
24, R_1 = O-(4-Me-Ph)
25, R_1 = NH-(4-CN-Ph)
26, R_1 = O-(4-CN-Ph)
27, R_1 = NH-(4-OMe-Ph)
28, R_1 = O-(4-OMe-Ph)
29, R_1 = NH-(4-OH-Ph)
30, R_1 = O-(4-OH-Ph)

Reagents and conditions: (a) aniline, 35% HCl, iPrOH, 80 °C, 1.5 h; (b) phenol, K_2CO_3, DMF, 140 °C, 12 h; (c) R_2-Bpin, Pd(PPh$_3$)$_4$, K_2CO_3, 1,4-dioxane/H_2O = 1:1, 120 °C, 1 h, μW; (d) R_2-Bpin, Pd(dppf)Cl$_2$, Cs_2CO_3, toluene/H_2O = 2:1, 90 °C, 12 h; after c or d, additional deprotection under TFA, DCM, rt, 1 h for **11, 14-30**.

Array at C7. To identify potent inhibitors, we initially focused our design attempts on the 4-aminoquinolone scaffold. First, we hypothesized that the overall activity of 4-aminoquinolone might be improved by introducing a suitable moiety into the molecule to establish additional π interactions with Gly1202 and hydrogen bonding or ionic interactions with polar amino acid residues at the solvent front. Based on our structural analysis, we planned to install a variety of (hetero)arene appendages at the C7 position to evaluate the substituent space of 4-aminoquinoline while the phenyl group at the C4 position remained fixed (Table 1). The resulting derivatives were subjected to a subsequent full IC$_{50}$ value determination. To the best of our knowledge, the 4-aminoquinoline scaffold is not present in any of the
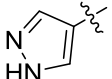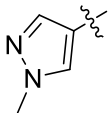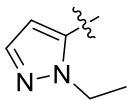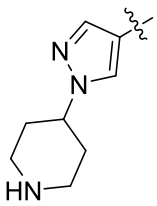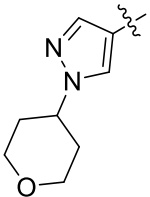
ALK inhibitors reported so far. The (hetero)arene groups at the 7 position seem to be stabilized in the internal region of the ATP-binding site because the chemical moiety group at the C7 position points to the center of the N-terminal domain in docking simulations (Figure 2). Of particular significance is the observation that a profound effect on potency was displayed upon the installation of the 4-(1H-pyrazol-1-yl)piperidine group. Molecular docking study of compounds **11** consistently indicated that the pyrazolyl piperidine moiety of the appendage plays an important role in determining activity by establishing a hydrogen bonding interaction with Glu1210. This effect is apparently one of the reasons for the better inhibitory activity of compounds bearing the pyrazolyl piperidine moiety.

Table 1. Exploration of groups at the C7 position of 4-phenylaminoquinoline derivatives.
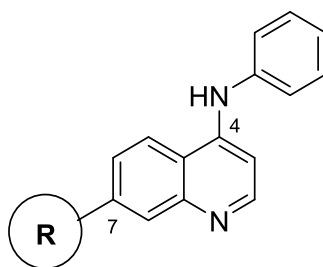
Compd.	R	IC$_{50}$ (µM)	
		WT	L1196M
1	H	147±29	112±33
2	Br	65.7±9.9	59.1±12.3
3		3.69±1.24	2.68±0.92
4		2.86±0.84	6.59±1.71
5		2.99±1.62	2.70±0.69
6		7.39±2.52	7.13±1.52

7		4.23±1.17	3.81±0.38
8		8.81±2.71	10.3±4.3
9		4.74±0.85	6.08±1.47
10		23.2±8.2	28.4±6.8
11		1.80±0.25	1.18±0.43
12		2.71±0.48	3.46±1.71
staurosporine		0.0019	0.00078

Identification of O-Linked Quinoline Scaffold. Although compound **11** is a newly identified

L1196M inhibitor with micromolar potency, we decided to make some modifications to the structural and

electrostatic features of 4-aminoquinoline scaffold to find more potent inhibitors with at least

submicromolar-level inhibitory activity. For the 4-aminoquinoline core, the acidic conditions can stabilize

the quinoline tautomer where the quinoline is readily protonated to give the quinolinium ion. From this

perspective, we speculated that errors in the binding modes and scoring function could occur from

underestimation of the tautomerism and protonation of the 4-aminoquinoline scaffold, which might be

invoked to explain, at least partly, the lower inhibitory activity. To determine the potential effect of the

tautomerism, the binding modes of 4-phenylaminoquinoline at different pH values were thoroughly

investigated with docking simulations. As depicted in Figure 2, we note that the quinoline tends to be

mostly protonated (marked with red dashed circle) in the physiologically relevant pH 6.5-8.5 range,

preventing the quinoline scaffold from establishing a hydrogen bond at the hinge region. The introduction

of the additional tautomerism and protonation factors seemed to guarantee better prediction accuracy of

the ligand binding affinity. Therefore, it would be reasonable to consider their electrostatic features to

design new inhibitors with increased potency. For this reason, we investigated the relevance of the effect

of ionization pH and inhibitory activity.
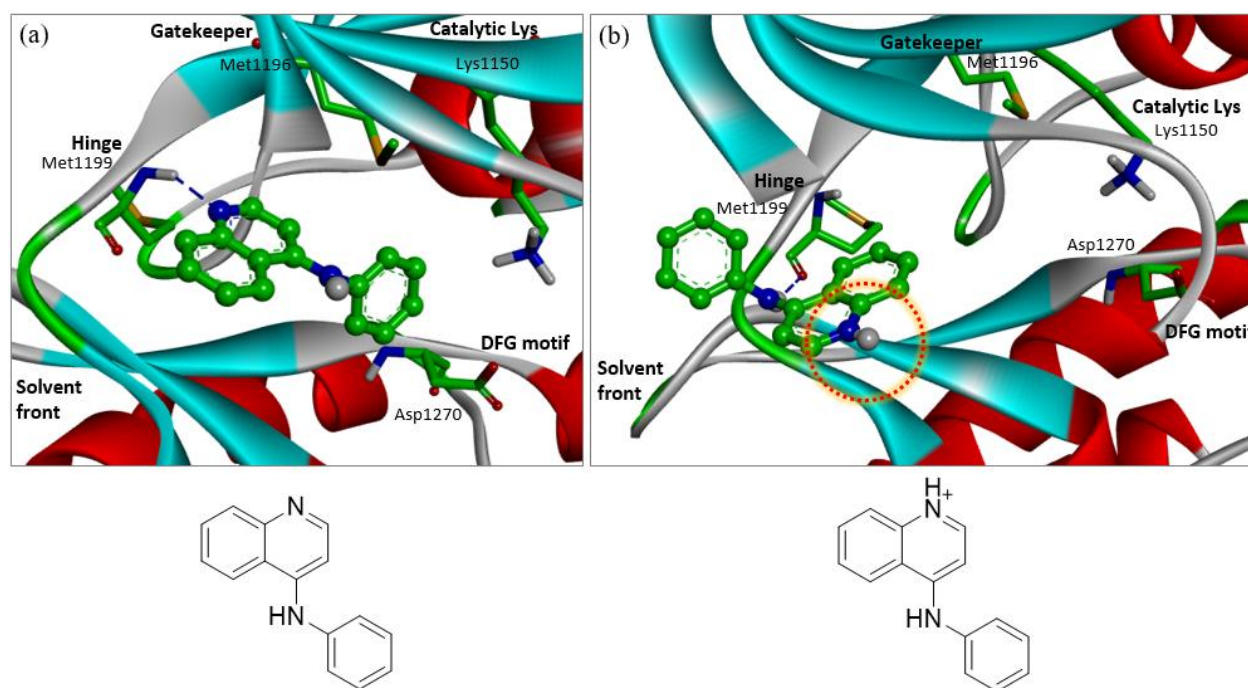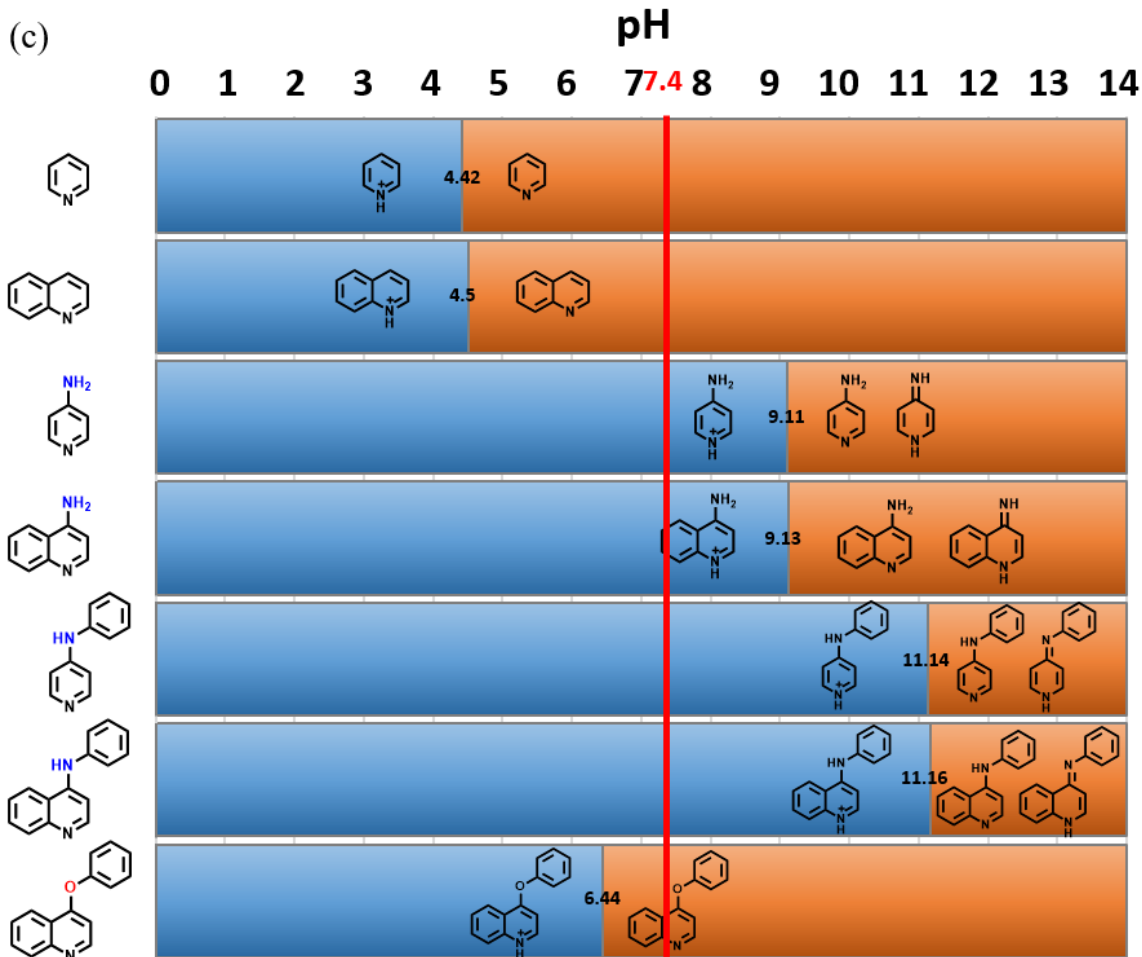
Figure 2. (a) Binding mode of 4-anilinoquinoline obtained through preparing inhibitors at pH above 11.16 followed by normal docking study (PDB: 2YFX). (b) Calculated binding mode of 4-phenylaminoquinoline at pH 6.5-8.5. Protonated site is marked with red dashed circle (PDB: 2YFX). (c) Ionization pH of each marked unit and existing form in the blue- and orange-colored pH ranges.

Figure 2c shows the ionization pH and range of each protonated/deprotonated form of the pyridine and quinoline derivatives calculated in the Discovery Studio program. By the resonance effect of the 4-aminopyridine moiety, the lone pair electron at N of the 4-amino group is transferred to the C-N bond at the C4 of quinoline to form an N-positively charged imine and delocalized to raise the electron density of the quinoline nitrogen. The ionization pH reaches 9.1 in both pyridine and quinoline, even higher in 4-phenylamino-substituted scaffolds, to cause the compounds to mostly exist in protonated form at physiological pH. We speculated that decreasing the resonance stability by replacing the amino linker

with an ether linkage would lower the ionization pH, and consequently, the deprotonated neutral form of 4-phenoxyquinoline scaffolds would be preferred. Indeed, the calculated ionization pH of 4-phenoxyquinoline is 6.44, revealing that the majority of this moiety exists in the neutral form so that the quinoline nitrogen is able to establish hydrogen bonding in the ATP-binding site. In addition, protonation and tautomerism can influence the structural length and bond rotatability of the compounds.[31] In this sense, the structure of the 4-phenoxyquinoline scaffold tends to be more flexible and could serve as a more effective surrogate for the corresponding 4-aminoquinoline core. To assess this hypothesis, the influence of protonation and tautomerism was investigated by changing the amino linkers along with studying the SAR profiles (Table 2).

To our delight, changing the linking moiety from NH in the 4-aminoquinoline scaffolds to O results in remarkable increases in the inhibitory activity. For example, the biochemical potency appears to increase by a factor of 40 in going from **23** (L1196M, IC_{50} = 129 nM) to **24** (L1196M, IC_{50} = 3.3 nM) due to the replacement of the amine linker with ether, the latter of which is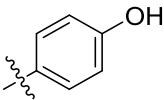 identified as the exclusively preferred linker (Table 2). This result indicates the importance of the neutral form of quinoline moieties, participating in a hydrogen bond with the hinge to effectively impair the enzymatic activity in the sense that the 4-alkoxyquinoline scaffold is more capable of acting as a hydrogen bond acceptor than the corresponding 4-aminoquinoline moiety. Next, various substituents can be introduced on the 4-phenoxy ring to maximize the binding affinity in the DFG motif in the A-loop and the nearby vacant binding pocket. As can be inferred from the similar IC_{50} values of **14**, **18** and **22**, various patterns of substitution are acceptable at the 4-phenoxy ring to achieve submicromolar inhibitory activity. The phenol group in **30** is likely to function as a hydrogen bond acceptor to Lys1150, as reflected by the excellent IC_{50} value (L1196M, IC_{50} = 7 nM). Therefore, it becomes apparent that the biochemical potency of quinolone-based L1196M mutant inhibitors can be augmented to the low nanomolar level by introducing an ether linkage. The inhibitory activity of **14** compared to **13** with a CH_2-linked moiety also indicates the superiority of the 4-phenoxy group as the optimal substructure for binding in mutant ALK (L1196M).

Table 2. Inhibition effects of quinoline scaffold attached with different linkages at C4.
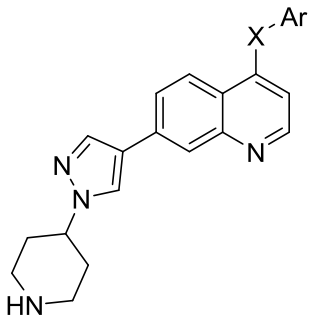
Compd.	Ar	X	IC$_{50}$ (nM)	
			WT	L1196M
11		NH	1,803±451	1,179±268
13		CH$_2$	288±43	242±26
14		O	126±32	118±18
15		NH	219±41	62±12
16		O	35.4±11.3	30.7±9.6
17		NH	377±150	504±201
18		O	155±42	58.8±11.3
19		NH	1,483±98	1,075±146
20		O	256±86	41.5±10.5
21		NH	181±34	58±11
22		O	148±30	26.3±7.4
23		NH	201±67	129±31
24		O	50.2±31.5	3.3±0.8
25		NH	1,664±420	926±241
26		O	231±69	93.5±31.2
27		NH	1,064±318	547±201
28		O	33.6±7.5	28.4±11.2

29		NH	26.4±7.3	50.9±14.5
30		O	5.2±1.4	7.1±2.3
staurosporine			1.7	0.67

Binding Mode Analysis of Inhibitor. To address structural and mechanistic aspects relevant to the potent inhibition by the newly identified inhibitors, we analyzed the interactions that stabilize the binding mode of inhibitors in the mutant ALK (L1196M) protein structure (PDB ID: 2YFX). The binding modes of **30** in the ATP-binding sites of the L1196M mutant is presented in Figure 3. The lowest-energy conformation shows the hydrogen bond formation between the N of quinoline and the backbone of Met1199, and this quinoline core is stabilized via hydrophobic interaction with the alkyl chain of Leu1122 and Ala1148 on the upper side and Leu1256 at the bottom of the pocket. A small pocket formed by Val1130, Met1196 and Lys1150 is occupied by a 56.1° tilted phenyl head group, and this hydroxyl group serves as an anchor by forming additional two hydrogen bonds with the two opposite-charged side chains of Lys1150 and Asp1270. Interestingly, a larger gatekeeper Met1196 residue was found at the interface formed by van der Waals contacts between the terminal phenoxy moiety and the ALK mutant (L1196M) (Figure 3). The piperidine on the inhibitor appeared to point toward the solvent front by forming a salt bridge with Glu1210 located on the outside of the kinase domain. Further stabilization may be achieved through the van der Waals contacts of its the pyrazole moiety with the hydrophobic side chains of Leu1122, Gly1201, Gly1202 and Ala1200. A similar binding mode would be speculated to occur in the cases of compounds **20**, **28** and **30**, which form interactions such as hydrogen bonding. The overall structural features derived from the docking simulations confirmed that the inhibitory activities of compound **30** were attributed to the multiple hydrogen bonds and hydrophobic interactions established simultaneously in the ATP-binding site of the L1196M mutant.
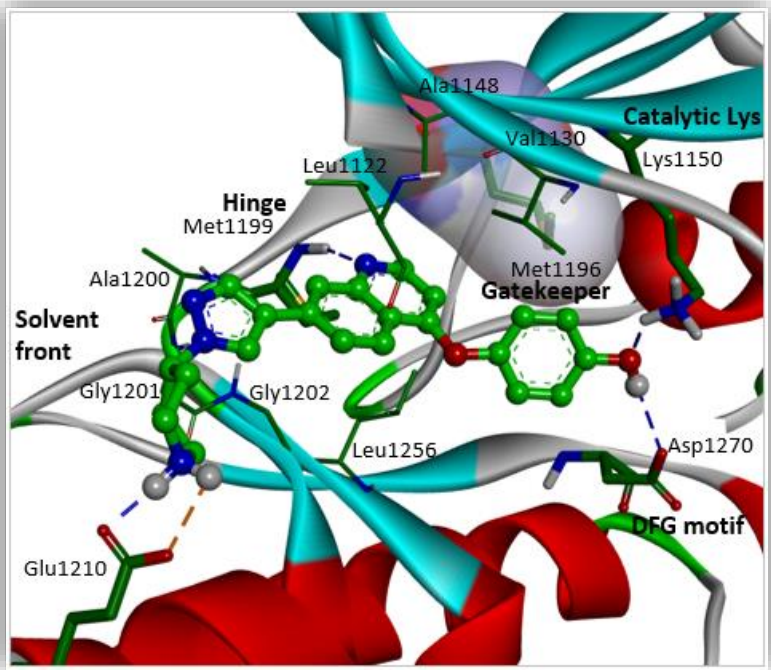
Figure 3. Calculated binding mode of **30** at the ATP binding site of ALK L1196M (PDB ID: 2YFX). Each dashed blue line and orange line indicates a hydrogen bond and salt bridge, respectively. Gatekeeper was displayed in semitransparent solid surface.

Mechanism of action (MOA) studies. To understand the interaction and binding modes of these inhibitors with ALK L1196M, mechanism of action (MOA) studies including ATP competition evaluation and K_i determination were performed. As shown in Figure 4, the progress curves are linear regardless of the amount of inhibitor, suggesting the inhibition by **24** is not time-dependent.
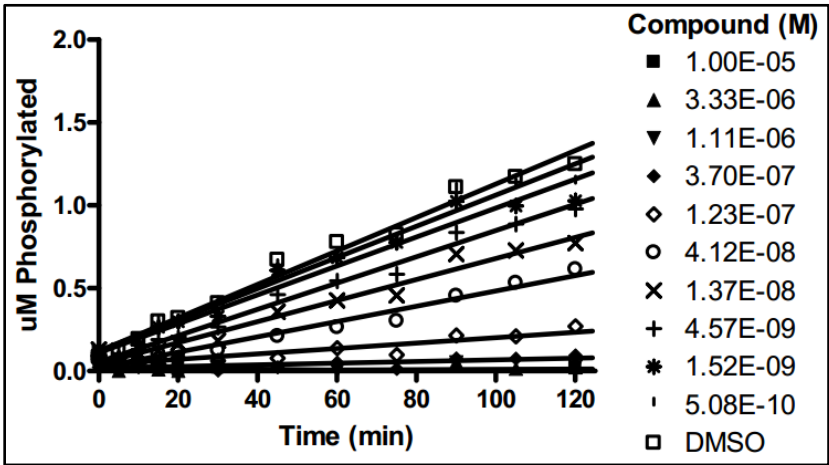
Figure 4. Progress Curves for ALK (L1196M) with **24**.

The apparent K_m is increased when inhibitor concentration is increased in Michaelis-Menten plot (Figure

5A) and all lines are converged on the Y-axis in the double-reciprocal plot (Figure 5B). As shown in the

Lineweaver-Burk plots (Figure 5B), **24** appears to impair the kinase activity of the mutant in the ATP-

competitive fashion.

A   Michaelis-Menten Plot for ALK (L1196M)

	DMSO	13.7 nM	41.2 nM	123 nM	370 nM
VMAX	0.04230	0.04401	0.04195	0.05810	0.05458
KM	30.94	58.76	94.60	298.0	859.8

B   Lineweaver-Burk Plot for ALK (L1196M)

	DMSO	13.7 nM	41.2 nM	123 nM	370 nM
Y-intercept when X=0.0	29.23 ± 5.415	33.35 ± 7.801	40.04 ± 7.001	51.82 ± 31.61	184.8 ± 225.9
X-intercept when Y=0.0	-0.04957	-0.03295	-0.02471	-0.01229	-0.01507
1/slope	0.001696	0.0009880	0.0006170	0.0002371	0.00008155

Figure 5. Michaelis-Menten Plot (A) and Lineweaver-Burk Plot (B) for ALK (L1196M) with **24**

When % enzymatic activities of slopes relative to that of DMSO control at each ATP concentration are

plotted against inhibitor concentration and draw IC_{50} curves, the IC_{50} values of **24** were increased when

ATP concentration was increased, as expected for common ATP-competitive inhibitors.
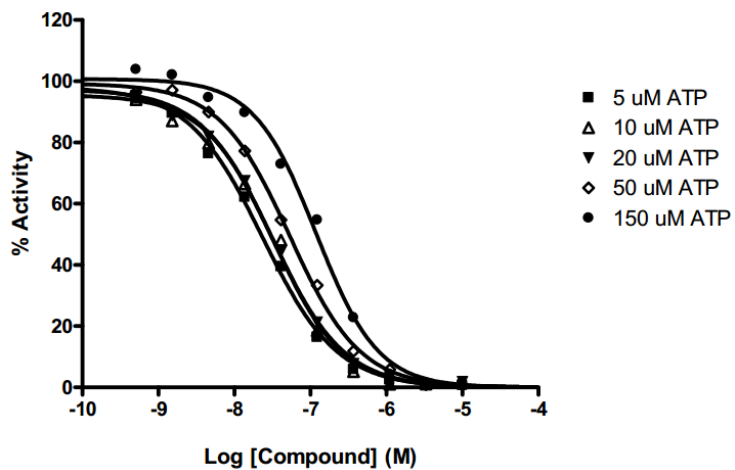
Figure 6. IC$_{50}$ curves for ALK (L1196M) at different ATP concentrations with **24**

Next, global fit was performed for **24** and results are listed in the table in Figure 7. The high value of *Ki'* (almost infinity) means the compound has very little affinity for enzyme/ATP complex, which turns ATP-competitive inhibition of ALK L1196M by **24**. The results from MOA studies show that **24** is not time-dependent and competitive with respect to ATP with the K_i value of 22 nM and K_m value of 32.6 μM.
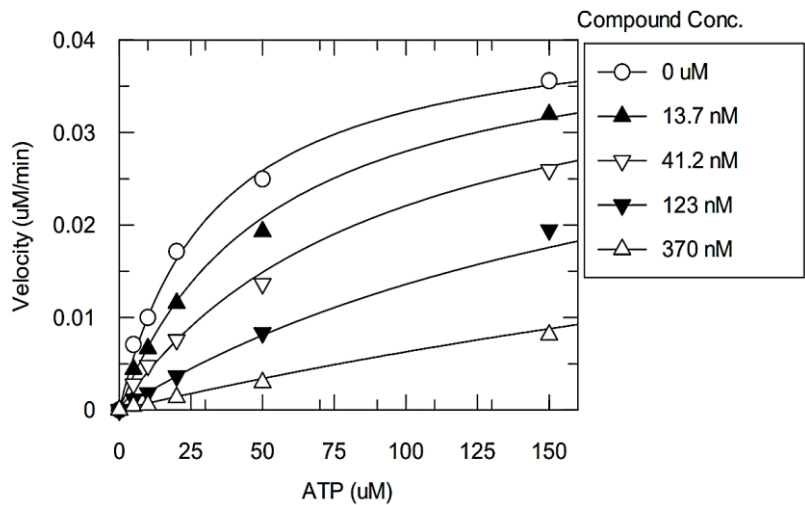
Parameter	Value	Std. Error
Vmax	0.0427	0.0010
K_m	32.5684 μM	2.1206
K_i	21.9872 nM	1.5171
K_i' value	4.08474e+019 nM	0.0000

Figure 7. IC$_{50}$ curves for ALK (L1196M) at different ATP concentrations with **24**.

ALK Mutant and Kinase Selectivity Profiling. As summarized in Table 3, compounds **24**, **28**, and **30** were tested against a panel of the most common secondary ALK mutants (L1196M, C1156Y, F1174L, G1269A, L1152R, G1202R).[13,26,32] Notably, compound **30** exhibited good potency against the secondary ALK mutants (L1196M, C1156Y, F1174L, G1269A, L1152R) with IC_{50} values ranging from 7 to 30 nM, although it showed an inhibitory activity against the G1202R mutant in the micromolar range.

Table 3. IC_{50} values of **24**, **28** and **30** against ALK mutants.

Compd.	IC_{50} (μM)					
	L1196M	C1156Y	F1174L	G1269A	L1152R	G1202R
24	0.0033	0.0409	0.141	0.0351	0.159	9.43
28	0.0284	0.0422	0.154	0.0384	0.155	8.91
30	0.0071	0.0115	0.0093	0.0162	0.0296	4.45
staurosporine	0.00073	0.0017	0.0016	0.00074	0.0029	0.0038

To obtain a detailed picture of the selectivity profile of this series, potent inhibitor **24** was further subjected to kinase selectivity profiling with a panel of 85 cancer related kinases on the kinome tree in a high-throughput binding assay at a concentration of 1 μM (see Table S1 in Supporting Information for more detail). Overall, **24** showed moderate to good specificity profiles, and kinases against which **24** demonstrated meaningful off-target activity percent of control (POC < 10) were ALK (POC = 2.3), AURKA (POC = 9.1), FLT3 (POC = 5.2), KIT (POC = 4.4), RET (POC = 3.3), TIE2 (POC = 4.9) and VEGFR2 (POC = 2.3). Other kinases inhibited by **24** are ACVR1B (POC = 14), LTK (POC = 13), FGFR1 (POC = 12), MEK2 (POC = 17) and MET (POC = 15).

Effect on Cell Proliferation and Cell-Signaling Downstream. This series of potent inhibitors were further tested for cellular growth inhibition against cancer cells. We tested cell viability assay with FDA approved ALK inhibitors (crizotinib, ceritinib and alectinib) along with the representative compound **30** against Ba/F3 EML4-ALK WT (EA WT) and Ba/F3 EML4-ALK L1196M (EA L1196M) cells. As shown in Figure 8a, crizotinib did not effectively inhibit cell proliferation of Ba/F3 EA L1196M cells while

crizotinib significantly inhibited proliferation in Ba/F3 EA WT cells. On the other hand, compound **30** effectively inhibited the cell growth and was comparable to ceritinib and alectinib against both wild type BaF3 EML4-ALK cells and BaF3 EML4-ALK cells with L1196M in a dose-dependent manner. [8,16, 33] Next, we carried out an evaluation of their antiproliferative activity on the H2228 and H2228 CR cell lines, the latter of which is crizotinib-resistant.[34] Next, H2228 and H2228 CR cells were treated with different doses of crizotinib for 72 h, and then MTT assays were performed. As expected, crizotinib significantly inhibited proliferation in H2228 crizotinib-sensitive cells (IC_{50} = 2.5 µM) but did not effectively inhibit cell proliferation of H2228 CR crizotinib-resistant cells (IC_{50} = 10 µM). In order to investigate whether **30** could overcome the resistance to crizotinib, H2228 CR cells were treated with different doses of crizotinib, ceritinib, alectinib and **30** for 72 h. The results from the MTT assay indicated that H2228 CR cells exhibited high resistance to crizotinib, whereas **30**, ceritinib, and alectinib effectively inhibited the cell growth of H2228 CR cells in a dose-dependent manner (Figure 8b).
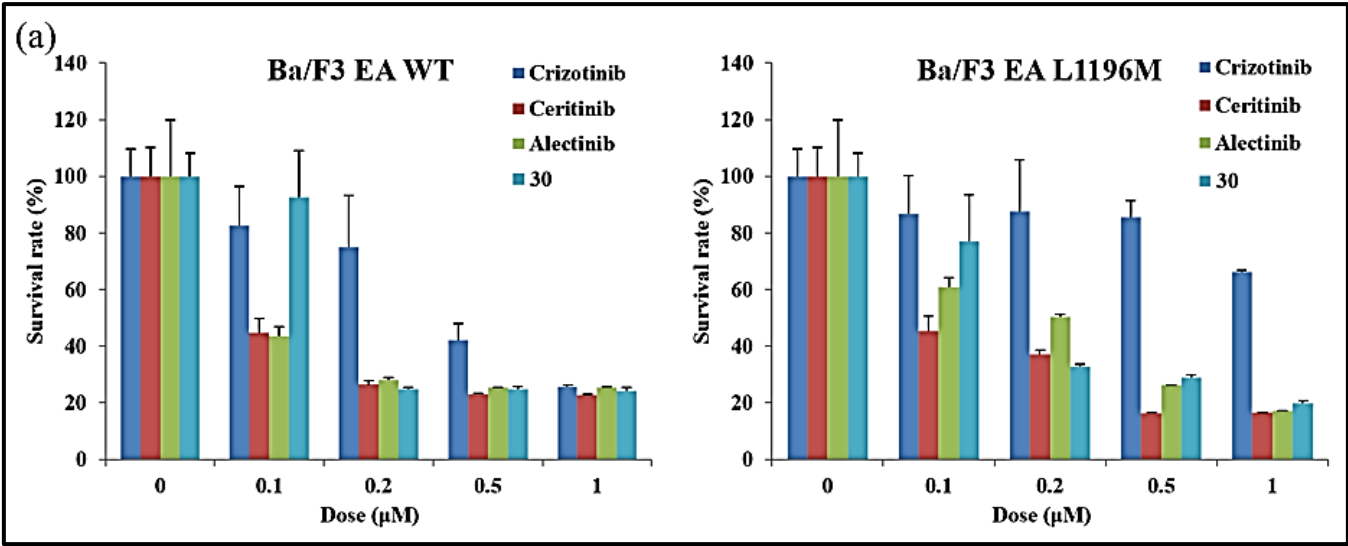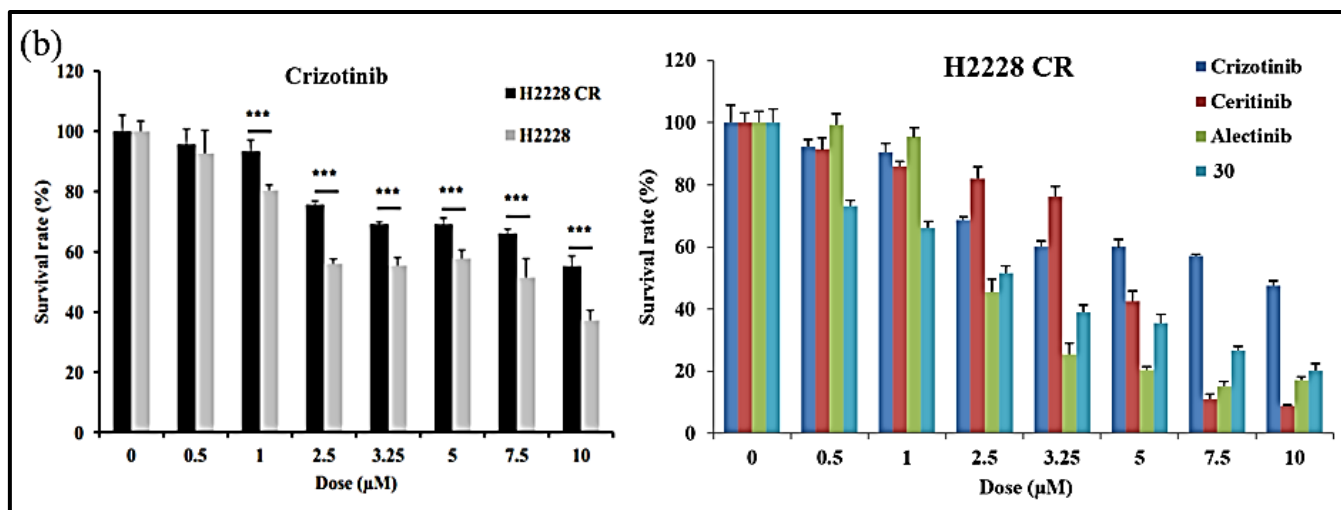
Figure 8. Cell viability of crizotinib, ceritinib, alectinib and **30**. Cell viability of crizotinib, ceritinib, alectinib and **30** were measured in (a) Ba/F3 EML4-ALK WT (EA WT), EML4-ALK L1196M (EA L1196M), H2228 and (b) H2228 CR human lung cancer cells by MTT assay. EA = EML4-ALK

To identify the molecular mechanism of **30** in overcoming acquired crizotinib resistance, we examined the effect of **30** on PI3K/AKT and MAPK signaling activation, which were reported to be not only the main downstream signaling pathways of ALK, but also the key mechanism for crizotinib resistance. In H2228 crizotinib-sensitive cells, crizotinib obviously inhibited the expression of p-AKT, downstream of PI3K/AKT signaling, but not p-ERK, downstream of MAPK signaling. However, **30** inhibited the expresssion of both p-AKT and p-ERK (Figure 9). More importantly, **30** remarkably inhibited the expression of both p-AKT and p-ERK in H2228 CR crizotinib-resistant cells, compared with crizotinib (Figure 9). Overall, these results showed that **30** successfully overcame crizotinib resistance by decreasing PI3K/AKT and MAPK signaling.
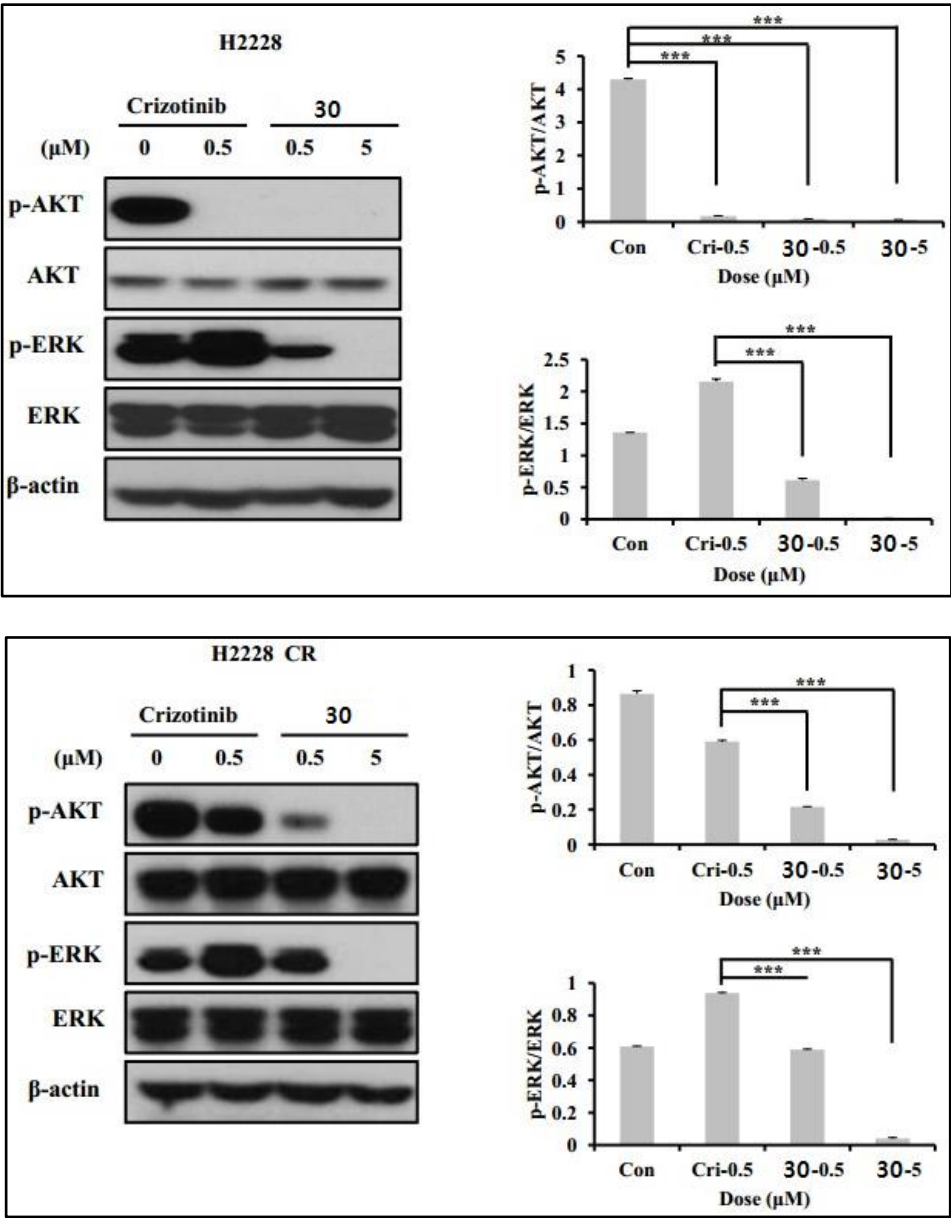
Figure 9. Compound **30** increased crizotinib sensitivity and overcame crizotinib resistance by decreasing PI3K/AKT and MAPK signaling in crizotinib-sensitive and -resistant human lung cancer cells. H2228 and H2228 CR human lung cancer cells were treated with the indicated concentrations of **30** and crizotinib for 3 h, and then the expression levels of p-AKT and p-ERK were measured by western blotting. Data are presented as means ± S.D. (***$P < 0.005$).

Two leading compounds **24** and **28** were subjected to pharmacokinetic studies. As shown in Table 4a, rat pharmacokinetic parameters were determined after oral administration and intravenous injection, which showed fair oral bioavailability (**24**: 44.8%, **28**: 45.5%, **30**: 24.8%). Next, we assessed the hERG

inhibition of representative compounds of this series, and IC_{50} values for **24**, **28**, and **30** were determined as shown in Table 4b. The assay is based on the competition of fluorescently labeled Tracer binding to the membrane preparation containing hERG. Compounds **24**, **28**, and **30** exhibited moderate inhibition of the hERG channel, with activities ranging from 2.46 to 3.12 µM.

Table 4. (a) Rat pharmacokinetic properties of compound **24** and **28** and (b) IC_{50} values of compounds **24**, **28**, and **30** against hERG.

(a)

Compd.		Dose (mg/kg)	$T_{1/2}$ (hr)	T_{max} (hr)	C_{max} (ng/mL)	AUC_{last} (hr*ng/mL)	F (%)
24	IV	1.0	3.3	0.1	94.1	166.0	
	PO	10.0		4.0	130.7	744.6	44.8
28	IV	1.0	10.7	0.1	48.9	95.9	
	PO	10.0		4.0	83.9	436.7	45.5
30	IV	1.0	3.5	0.1	83.5	155.1	
	PO	10.0		6.0	78.4	384.0	24.8

(b)

	24	**28**	**30**	**E-4031**
hERG IC_{50} (µM)	3.12	2.46	2.76	0.0012

CONCLUSION

By fragment based drug design and modification followed by analysis of chemical properties, we identified 4-phenoxyquinoline derivatives as ALK and ALK L1196M inhibitors. Starting from the 4-aminoquinoline moiety, a fragment-growing strategy was adopted to promote hydrophobic interaction, solvation effect and advanced interactions. The electrostatic properties of molecular structures in physiological conditions were carefully considered for the structural design of inhibitors. In the range of physiological pH conditions, electron delocalization from the 4-aminogroup to the quinoline nitrogen is likely to lead to protonation of the 4-aminoquinoline moiety that blocks the quinoline nitrogen from binding the hinge amino acid backbone. The scaffold was redesigned to eliminate this problematic

character, altering the linker from NH to O. The enzymatic inhibition of ALK L1196M dramatically increased, especially in the case of 4-phenoxyquinoline bearing *p*-substitutuent, whose binding stability is demonstrated in the docking model. The new inhibitors exhibited significant antiproliferative effects on H2228 CR crizotinib-resistant cells by inhibiting the expression of both p-AKT and p-ERK. These results show the advantages of the 4-phenoxyquinoline moiety and have considerable implications for the drug design. Further studies to increase cellular potency by modifying cellular permeability and water-solubility are currently in progress.

EXPERIMENTAL SECTION

General Methods and Materials. Unless stated otherwise, reactions were performed in a flame-dried glassware under positive pressure of nitrogen using freshly distilled solvents. Analytical thin layer chromatography (TLC) was performed on precoated silica gel 60 F_{254} plates, and visualization on TLC was achieved via UV light (254 and 354nm). μW irritation was conducted by Anton Paar Microwave 300 single-mode microwave synthesis reactor. Flash column chromatography was utilized on silica gel (400-630 mesh). ^{1}H NMR was recorded on 600MHz, 400MHz or 300 MHz and chemical shifts were quoted in parts per million (ppm) referenced to the appropriate solvent peak or 0.0 ppm for tetramethylsilane. The following abbreviations were used to describe the peak splitting patterns when appropriate: br = broad, s = singlet, d = doublet, t = triplet, q = quartet, m = multiplet, dd = doublet of doublet. Coupling constants, *J*, were reported in hertz unit (Hz). ^{13}C NMR was recorded on 100 MHz or 150MHz and was fully decoupled by broad band proton decoupling. Chemical shifts were reported in ppm referenced to the center line of a triplet at 77.0 ppm of chloroform-*d*. Mass spectral data were obtained from the KAIST Basic Science Institute by Bruker Daltonik HR-MS using the EI method or Agilent LR-MS. High-performance liquid chromatography analyses for checking mass spectral data (using EI method) of synthesized compounds were performed on a Agilent HPLC equipped with an Agilent Poroshell 120 EC-C18 reverse phase column (4.6 × 50 mm, 2.7 Micron) and by quadrupole LC/MS. The mobile phase was a mixture of MeOH (0.1% TFA) and H_2O (0.1% TFA). Compound purity was determined by integrating

the peak areas of liquid chromatogram, monitored at 254 nm. Flow rate (0.5 mL/min). Gradient system: from MeOH (0.1 % TFA) 10% and H_2O (0.1% TFA) 90% (0 min) to MeOH (0.1% TFA) 90% and H_2O (0.1% TFA) 10% (18 min), the solvent ratio was maintained for 23 min; the solvent ratio was changed to MeOH (0.1% TFA) 10% and H_2O (0.1% TFA) 90% (25 min). All final compounds were found to have >95% purity. Commercial grade reagents and solvents were used without further purification except as indicated below. Unless stated otherwise, all commercial grade reagents and solvents were used without additional purification.

Preparation of Compounds

Preparation of Boron Coupling Partners for Suzuki Coupling.

R_2-Bpin (4,4,5,5-tetramethyl-1,3,2-dioxaborolane substituted compounds) reagents for Suzuki coupling (GP I-2 and II-2) were prepared by synthesis of iodo-substituted intermediates followed by miyaura borylation in the case of **11**-**30**. To synthesize **3**-**10**, commercially available boronic acid or Bpin-substituted reagents were used. Preparation of synthesized boron reagents were proceeded through reported synthetic procedures in *J. Med. Chem.* **2011**, *54*, 6342–6363 (synthesis of **68**). In the case of R_2-Bpin reagents for **12**, 1-(tetrahydro-2*H*-pyran-4-yl)-4-(4,4,5,5-tetramethyl-1,3,2-dioxaborolan-2-yl)-1*H*-pyrazole was prepared by following procedure: A solution of 4-iodo-1-(tetrahydro-2*H*-pyran-4-yl)-1*H*-pyrazole (95.5 mg, 0.3434 mmol) in anhydrous THF (1 mL) was cooled to 0 °C under an atmosphere of N_2. 2 M *i*PrMgCl solution in THF (0.26 mL, 0.5151 mmol) was added dropwise for 10 min, and the mixture was stirred at rt for 1 h. To the reaction mixture at 0 °C was added 2-methoxy-4,4,5,5-tetramethyl-1,3,2-dioxaborolane (87.2 μL, 0.5323 mmol) and the resulting mixture was stirred at rt overnight. The reaction was quenched with saturated NaCl (aq.) at 0 °C, and the mixture was extracted with EtOAc (100 mL x 3). The organic layers were dried over Na_2SO_4, filtered, and concentrated under redused pressure. The residue was directly used for Suzuki coupling without further purification.

General Procedure (GP) I-1 for the Synthesis of Compounds 1, 2 and 3 and 7-bromo-*N*-phenylquinolin-4-amine Intermediates.

In a round bottom flask, 7-bromo-4-chloroquinoline (0.092 mmol) and aniline (0.10 mmol) were dissolved in 1 mL of *i*PrOH. A catalytic amount (1 drop) of 35% hydrochloric acid was added to this mixture at room temperature and the final mixture was stirred for 2 h at 80 °C. The reaction mixture was cooled to room temperature, and the precipitate was filtered with *i*PrOH when the precipitate is observed in the crude mixture. When the whole materials are solved in the solvent after reaction, the solvent was evaporated and small portion of diethyl ether was added to precipitate product from mixture. The precipitate was filtered with diethyl ether, and the solid was dried under reduced pressure obtaining products or intermediates that was submitted to the next reaction without further purification. (*J. Med. Chem.* **2014**, *57*, 701−713)

General Procedure I-2 for Suzuki Coupling of 4-anilinoquinoline Substrates.

The mixture of 7-bromo-*N*-phenylquinolin-4-amine substrate **2** (0.0334 mmol), proper boronic ester or boronic acid reagent (0.100 mmol), Pd(PPh$_3$)$_4$ (0.0033 mmol) and K$_2$CO$_3$ (0.100 mmol) in dioxane:H$_2$O (=1:1, 2 mL) was stirred for 1 h at 120 °C under μW irradiation. EtOAc and H$_2$O were added to the mixture and the organic materials were extracted with EtOAc (50 mL x 3), followed by dring with MgSO$_4$. Filtered solution was concentrated under reduced pressure and purified on flash column chromatography (dichloromethane/methanol = 20:1) to give desired product. If inseparable impurity is observed, further purification was proceded by flash column chromatography (EtOAc/diethyl ether = 20:1). If necessary, boc deprotection was proceded in the DCM (0.5 mL) solution of product. At 0 °C, trifluoroacetic acid (0.3 mL) was added dropwise and the resulted mixture was stirred at room temperature for 1 h. The solvent was evaporated under *vacuo*, and washed with diethyl ether (1 mL x 3) to give pure product as the TFA salt.

General Procedure II-1 for the Synthesis of 7-bromo-4-phenoxyquinoline Intermediates.

7-bromo-4-phenoxyquinoline. 7-bromo-4-chloroquinoline (15.0 mg, 0.0623 mmol), phenol (5.9 mg, 0.062 mmol), and K_2CO_3 (21.5 mg, 0.156 mmol) were placed in a round bottom flask. The reagent mixture was dissolved in *N, N*-Dimethylformamide under N_2 atmosphere and the reaction mixture was stirred overnight at 140 ℃. After cooling to room temperature, the mixture was diluted with EtOAc and H_2O, and the organic materials were extracted with EtOAc (50 mL x 3). The combined organic phases were dried over anhydrous $MgSO_4$ and filtered. The organic layer was concentrated under reduced pressure and purified on flash column chromatography (dichloromethane/methanol = 40:1) to give desired product as a pale yellow solid (15.0 mg, 80%). ^{1}H NMR (400 MHz, methanol-d_4) δ 8.60 (d, *J* = 5.3 Hz, 1H), 8.29 (d, *J* = 8.9 Hz, 1H), 8.17 (s, 1H), 7.74 (d, *J* = 8.9 Hz, 1H), 7.56 – 7.51 (m, 2H), 7.40 – 7.32 (m, 1H), 7.29 – 7.23 (m, 2H), 6.61 (d, *J* = 5.4 Hz, 1H). (*Bioorg. Med. Chem.* **2005**, *13*, 1069–1081)

General Procedure II-2 for Suzuki Coupling of 4-phenoxyquinoline Substrates.

The mixture of 7-bromo-4-phenoxyquinoline substrate (0.0500 mmol), *tert*-butyl 4-(4-(4,4,5,5-tetramethyl-1,3,2-dioxaborolan-2-yl)-1*H*-pyrazol-1-yl)piperidine-1-carboxylate as a boronic ester reagent (0.060 mmol), Pd(dppf)Cl$_2$.CH$_2$Cl$_2$ (0.0025 mmol) and Cs$_2$CO$_3$ (0.165 mmol) in toluene:H$_2$O (=2:1, 1.5 mL) was stirred overnight at 90 ºC. H$_2$O were added and the extraction was conducted with EtOAc (50 mL x 3). The combined organic phases were dried over anhydrous MgSO$_4$, filtered and concentrated. The residue was purified on flash column chromatography (DCM/MeOH = 40:1) to give desired product. Inseparable impurity was purified with flash column chromatography (diethyl ether/EtOAc = 1:20). Additional deprotection of boc group was conducted with the solution of product in DCM (0.5 mL) in a 10 mL round bottom flask. After cooling to 0 ºC, trifluoroacetic acid (0.3 mL) was added dropwise and the resulted mixture was stirred at room temperature for 1 h. The solvent was evaporated under *vacuo*, and washed with diethyl ether (1 mL x 3) to give desired product as the TFA salt.

***N*-phenylquinolin-4-amine (1).** Compound **1** was prepared (11.7 mg, pale yellow solid, 58% yield) according to GP I-1 from 4-chloroquinoline (15.0 mg, 0.092 mmol) and aniline (9.2 μL, 0.10 mmol) as a

starting material. ^{1}H NMR (400 MHz, methanol-d_4) δ 8.35 (d, J = 5.8 Hz, 1H), 8.31 (d, J = 7.4 Hz, 1H), 7.88 (d, J = 8.5 Hz, 1H), 7.72 (dd, J = 8.4, 6.9 Hz, 1H), 7.58 − 7.49 (m, 1H), 7.47 − 7.33 (m, 4H), 7.21 (t, J = 7.2 Hz, 1H), 6.92 (d, J = 5.5 Hz, 1H). ^{13}C NMR (150 MHz, methanol-d_4) δ 151.3, 150.8, 149.2, 141.4, 131.0, 130.6, 128.7, 126.3, 126.0, 124.7, 122.7, 121.0, 102.2. HRMS (ESI$^+$) m/z calcd. $C_{15}H_{13}N_2^+$ [M+H]$^+$: 221.1073, found: 221.1076.

7-bromo-*N*-phenylquinolin-4-amine (2). Compound **2** was prepared (171.4 mg, yellow solid, 93%) according to GP I-1 from 7-bromo-4-chloroquinoline (150 mg, 0.619 mmol) and aniline (62.1 μL, 0.680 mmol) as a starting material. ^{1}H NMR (400 MHz, methanol-d_4) δ 8.51 (d, J = 9.1 Hz, 1H), 8.37 (d, J = 7.1 Hz, 1H), 8.14 (s, 1H), 7.93 (d, J = 9.1 Hz, 1H), 7.60 (td, J = 7.3, 1.7 Hz, 2H), 7.53 − 7.41 (m, 3H), 6.89 (d, J = 7.1 Hz, 1H). ^{13}C NMR (150 MHz, methanol-d_4) δ 157.6, 144.1, 140.6, 138.1, 131.9, 131.3, 129.7, 129.4, 126.7, 126.1, 123.7, 117.6, 101.6. HRMS (ESI$^+$) m/z calcd. $C_{15}H_{12}BrN_2^+$ [M+H]$^+$: 299.0178, found: 299.0193.

Compounds **3-10** and **12** were prepared by using a same procedure described for the synthesis of **2** as a GP I-1, followed by similar procedure to GP I-2.

***N*,7-diphenylquinolin-4-amine (3).** Compound **3** was prepared (4.6 mg, pale yellow solid, 2 steps 29% yield) according to GP I. ^{1}H NMR (600 MHz, DMSO-d_6) δ 9.19 (s, 1H), 8.52 (d, J = 8.9 Hz, 1H), 8.49 (d, J = 5.4 Hz, 1H), 8.14 (s, 1H), 7.91 (d, J = 8.7 Hz, 1H), 7.87 (d, J = 7.6 Hz, 2H), 7.55 (t, J = 7.6 Hz, 2H), 7.45 (t, J = 7.6 Hz, 3H), 7.40 (d, J = 7.8 Hz, 2H), 7.18 (t, J = 7.3 Hz, 1H), 6.93 (d, J = 5.4 Hz, 1H). ^{13}C NMR (150 MHz, DMSO-d_6) δ 150.6, 148.5, 148.1, 141.1, 140.3, 139.2, 129.4, 129.1, 128.1, 127.0, 125.6, 124.0, 123.7, 123.1, 122.6, 118.7, 101.4. HRMS (ESI$^+$) m/z calcd. $C_{21}H_{17}N_2^+$ [M+H]$^+$: 297.1386, found: 297.1409.

***N*-phenyl-7-(pyridin-4-yl)quinolin-4-amine (4).** Compound **4** was prepared (3.9 mg, pale yellow solid, 2 steps 24% yield) according to GP I. ^{1}H NMR (600 MHz, DMSO-d_6) δ 9.09 (s, 1H), 8.70 (d, J = 5.1 Hz, 2H), 8.54 (d, J = 8.8 Hz, 1H), 8.52 (d, J = 5.3 Hz, 1H), 8.30 (s, 1H), 7.98 (d, J = 8.6 Hz, 1H), 7.92 (d, J =

4.9 Hz, 2H), 7.44 (t, J = 7.7 Hz, 2H), 7.39 (d, J = 7.8 Hz, 2H), 7.17 (t, J = 7.3 Hz, 1H), 6.96 (d, J = 5.3 Hz, 1H). ^{13}C NMR (150 MHz, DMSO-d_6) δ 151.5, 150.4, 149.2, 147.7, 146.2, 140.34, 137.7, 129.4, 127.1, 123.9, 123.4, 122.9, 122.5, 121.5, 120.0, 101.9. HRMS (ESI[+]) m/z calcd. $C_{20}H_{16}N_3^+$ [M+H][+]: 298.1339, found: 298.1362.

7-(6-aminopyridin-3-yl)-*N*-phenylquinolin-4-amine (5). Compound **5** was prepared (4.2 mg, ivory solid, 2 steps 25% yield) according to GP I. ^{1}H NMR (400 MHz, chloroform-*d,* methanol-*d4* cosolvent) δ 8.37 (d, J = 5.5 Hz, 1H), 8.32 (s, 1H), 8.05 (d, J = 8.6 Hz, 1H), 8.00 (s, 1H), 7.81 (d, J = 8.7 Hz, 1H), 7.63 (d, J = 8.7 Hz, 1H), 7.36 (t, J = 7.7 Hz, 2H), 7.28 (s, 2H), 7.14 (t, J = 7.3 Hz, 1H), 6.88 (d, J = 5.5 Hz, 1H), 6.60 (d, J = 8.5 Hz, 1H). ^{13}C NMR (100 MHz, DMSO-d_6) δ 159.6, 151.0, 149.6, 147.5, 146.3, 140.6, 138.8, 135.6, 129.3, 124.1, 123.6, 122.9, 122.6, 122.3, 122.2, 118.2, 108.1, 101.2. HRMS (ESI[+]) m/z calcd. $C_{20}H_{17}N_4^+$ [M+H][+]: 313.1448, found: 313.1458.

7-(furan-2-yl)-*N*-phenylquinolin-4-amine (6). Compound **6** was prepared (7.7 mg, yellowish brown solid, 2 steps 50% yield) according to GP I. ^{1}H NMR (400 MHz, DMSO-d_6) δ 9.32 (s, 1H), 8.49 (d, J = 8.9 Hz, 1H), 8.46 (d, J = 5.7 Hz, 1H), 8.14 (s, 1H), 7.94 (d, J = 8.8 Hz, 1H), 7.88 (dd, J = 1.8, 0.7 Hz, 1H), 7.53 – 7.42 (m, 2H), 7.42 – 7.35 (m, 2H), 7.25 (dd, J = 3.5, 0.8 Hz, 1H), 7.20 (tt, J = 7.2, 1.4 Hz, 1H), 6.87 (d, J = 5.6 Hz, 1H), 6.69 (dd, J = 3.4, 1.8 Hz, 1H). ^{13}C NMR (150 MHz, DMSO-d_6) δ 152.1, 149.8, 148.9, 144.0, 139.8, 131.5, 129.5, 124.5, 123.3, 123.0, 121.0, 120.6, 118.2, 112.5, 108.2, 101.2. HRMS (ESI[+]) m/z calcd. $C_{19}H_{15}N_2O^+$ [M+H][+]: 287.1179, found: 287.1199.

***N*-phenyl-7-(thiophen-2-yl)quinolin-4-amine (7).** Compound **7** was prepared (6.3 mg, white solid, 2 steps 39% yield) according to GP I. ^{1}H NMR (400 MHz, chloroform-*d,* methanol-*d4* cosolvent) δ 8.35 (d, J = 5.5 Hz, 1H), 8.11 (s, 1H), 8.08 (d, J = 8.8 Hz, 1H), 7.73 (d, J = 8.8 Hz, 1H), 7.49 (dd, J = 3.6, 1.1 Hz, 1H), 7.38 (dd, J = 8.5, 7.3 Hz, 2H), 7.34 (dd, J = 5.1, 1.1 Hz, 1H), 7.32 – 7.26 (m, 2H), 7.19 – 7.13 (m, 1H), 7.10 (dd, J = 5.1, 3.6 Hz, 1H), 6.89 (d, J = 5.5 Hz, 1H). ^{13}C NMR (100 MHz, chloroform-*d,* methanol-*d4* cosolvent) δ 150.9, 148.9, 148.8, 143.3, 139.9, 135.8, 129.7, 128.4, 126.0, 124.8, 124.5, 124.5, 123.6, 123.1, 121.6, 119.0, 101.8. HRMS (ESI[+]) m/z calcd. $C_{19}H_{15}N_2S^+$ [M+H][+]: 303.0950, found: 303.0975.

N-phenyl-7-(1*H*-pyrazol-4-yl)quinolin-4-amine (8). Compound **8** was prepared (6.6 mg, white solid, 2 steps 43% yield) according to GP I. ^{1}H NMR (400 MHz, DMSO-d_6) δ 13.06 (s, 1H), 8.93 (s, 1H), 8.42 (d, J = 5.3 Hz, 1H), 8.36 (d, J = 8.8 Hz, 2H), 8.14 (s, 1H), 8.09 (s, 1H), 7.83 (d, J = 8.7 Hz, 1H), 7.47 − 7.30 (m, 4H), 7.14 (tt, J = 7.1, 1.5 Hz, 1H), 6.86 (d, J = 5.3 Hz, 1H). ^{13}C NMR (150 MHz, DMSO-d_6) δ 150.9, 149.6, 147.5, 140.6, 136.7, 133.8, 129.3, 126.3, 123.6, 123.6, 122.9, 122.6, 122.4, 120.6, 117.9, 101.0. HRMS (ESI$^+$) m/z calcd. $C_{18}H_{15}N_4^+$ [M+H]$^+$: 287.1291, found: 287.1302.

7-(1-methyl-1*H*-pyrazol-4-yl)-N-phenylquinolin-4-amine (9). Compound **9** was prepared (12.4 mg, pale yellow solid, 2 steps 76% yield) according to GP I. ^{1}H NMR (600 MHz, DMSO-d_6) δ 9.12 (s, 1H), 8.42 (d, J = 5.4 Hz, 1H), 8.40 (d, J = 8.8 Hz, 1H), 8.37 (s, 1H), 8.07 (s, 1H), 8.03 (s, 1H), 7.80 (d, J = 8.7 Hz, 1H), 7.43 (t, J = 7.7 Hz, 2H), 7.38 (d, J = 7.8 Hz, 2H), 7.17 (t, J = 7.3 Hz, 1H), 6.85 (d, J = 5.5 Hz, 1H), 3.91 (s, 3H). ^{13}C NMR (150 MHz, DMSO-d_6) δ 150.2, 148.6, 148.1, 140.3, 136.6, 133.9, 129.4, 128.7, 123.9, 122.9, 122.8, 122.6, 122.6, 121.2, 117.7, 100.9, 38.8. HRMS (ESI$^+$) m/z calcd. $C_{19}H_{17}N_4^+$ [M+H]$^+$: 301.1448, found: 301.1467.

7-(1-ethyl-1*H*-pyrazol-5-yl)-N-phenylquinolin-4-amine (10). Compound **10** was prepared (8.1 mg, pale yellow solid, 2 steps 48% yield) according to GP I. ^{1}H NMR (400 MHz, DMSO-d_6) δ 9.09 (s, 1H), 8.57 − 8.45 (m, 2H), 7.93 (s, 1H), 7.64 (d, J = 8.7 Hz, 1H), 7.57 (d, J = 1.8 Hz, 1H), 7.44 (dd, J = 8.5, 7.1 Hz, 2H), 7.41 − 7.34 (m, 2H), 7.20 − 7.12 (m, 1H), 6.96 (d, J = 5.3 Hz, 1H), 6.54 (d, J = 1.8 Hz, 1H), 4.25 (q, J = 7.2 Hz, 2H), 1.35 (t, J = 7.2 Hz, 3H). ^{13}C NMR (100 MHz, DMSO-d_6) δ 151.5, 148.8, 147.7, 141.7, 140.4, 138.3, 131.1, 129.4, 128.4, 124.8, 123.9, 123.0, 122.5, 119.3, 106.5, 101.9, 44.3, 15.5. HRMS (ESI$^+$) m/z calcd. $C_{20}H_{19}N_4^+$ [M+H]$^+$: 315.1604, found: 315.1627.

N-phenyl-7-(1-(piperidin-4-yl)-1*H*-pyrazol-4-yl)quinolin-4-amine (11). Compound **11** was prepared (11.1 mg, pale yellow solid, 3 steps 69% yield) according to GP I. ^{1}H NMR (400 MHz, methanol-d_4) δ 8.55 (d, J = 8.8 Hz, 1H), 8.43 (s, 1H), 8.32 (d, J = 7.1 Hz, 1H), 8.16 (s, 1H), 8.09 − 7.93 (m, 2H), 7.59 (dd, J = 8.4, 7.1 Hz, 2H), 7.52 − 7.22 (m, 3H), 6.84 (d, J = 7.0 Hz, 1H), 4.67 (dt, J = 9.8, 4.8 Hz, 1H), 3.88 − 3.52 (m, 2H), 3.28 − 3.16 (m, 2H), 2.47 − 2.18 (m, 4H). ^{13}C NMR (150 MHz, methanol-d_4) δ 155.7,

142.1, 139.4, 138.7, 137.3, 137.0, 129.8, 127.7, 127.4, 125.3, 125.1, 123.4, 120.5, 115.5, 114.1, 99.4, 55.8, 42.7, 28.7. HRMS (ESI$^+$) m/z calcd. $C_{23}H_{24}N_5^+$ [M+H]$^+$: 370.2026, found: 370.2070.

N-phenyl-7-(1-(tetrahydro-2H-pyran-4-yl)-1H-pyrazol-4-yl)quinolin-4-amine (12). Compound **12** was prepared (7.8 mg, pale yellow solid, 2 steps 30% yield) according to GP I. ^{1}H NMR (600 MHz, DMSO-d_6) δ 9.08 (s, 1H), 8.51 (s, 1H), 8.42 (d, J = 5.4 Hz, 1H), 8.39 (d, J = 8.8 Hz, 1H), 8.11 (s, 1H), 8.07 (s, 1H), 7.83 (d, J = 8.7 Hz, 1H), 7.43 (t, J = 7.9 Hz, 2H), 7.38 (d, J = 7.8 Hz, 2H), 7.20 – 7.11 (m, 1H), 6.85 (d, J = 5.3 Hz, 1H), 4.45 (tt, J = 10.4, 4.7 Hz, 1H), 4.05 – 3.91 (m, 2H), 3.50 (td, J = 11.6, 2.6 Hz, 2H), 2.11 – 1.91 (m, 4H). ^{13}C NMR (150 MHz, DMSO-d_6) δ 150.3, 148.8, 148.0, 140.3, 136.3, 133.9, 129.4, 125.9, 123.9, 122.8, 122.8, 122.7, 122.6, 120.9, 117.8, 100.9, 65.9, 57.4, 32.9. HRMS (ESI$^+$) m/z calcd. $C_{23}H_{23}N_4O^+$ [M+H]$^+$: 371.1866, found: 371.1872.

Procedure for the Synthesis of 4-benzyl-7-(1-(piperidin-4-yl)-1H-pyrazol-4-yl)quinoline (13).

Step 1. The mixture of 7-methoxyquinolin-4-ol (100 mg, 0.57 mmol) and phosphoryl tribromide (1.7 g, 5.9 mmol) was heated to 110 ºC for 3 h. The reaction mixture was dropped in ice water and the mixture was basified with NH$_4$OH to pH 8 and extraction proceeded with EtOAc several times. The combined organic phases were dried over anhydrous MgSO$_4$, filtered, and concentrated. The residue was purified with flash column chromatography (EtOAc/hexane = 1:3 to 1:1) to give 4-bromo-7-methoxyquinoline (white solid, 97.3 mg, 72%). ^{1}H NMR (400 MHz, chloroform-d) δ 8.55 (d, J = 4.9 Hz, 1H), 8.03 (d, J = 9.2 Hz, 1H), 7.52 (d, J = 4.8 Hz, 1H), 7.39 (s, 1H), 7.25 (d, J = 9.3 Hz, 1H), 3.95 (s, 3H).

Step 2. A solution of 4-bromo-7-methoxyquinoline (20.0 mg, 0.0840 mmol), 2-benzyl-4,4,5,5-tetramethyl-1,3,2-dioxaborolane (22.4 μL, 0.1008 mmol), K$_2$CO$_3$ (34.8 mg, 0.252 mmol), and Pd(PPh$_3$)$_4$ (4.9 mg, 0.0042 mmol) in 1,4-dioxane:H$_2$O = 4:1 (1.25 mL) was heated to 100 °C for 6 h in a sealed tube. The resulting mixture was cooled to rt, and extracted with EtOAc. The combined organic layer was dried with MgSO$_4$ and concentrated in vacuo. The residue was purified with flash column chromatography (hexane/EtOAc = 1:1) to give 4-benzyl-7-methoxyquinoline (colorless oil, 13.4 mg, 64%). ^{1}H NMR (600

MHz, chloroform-*d*) δ 8.74 (d, *J* = 4.5 Hz, 1H), 7.91 (d, *J* = 9.2 Hz, 1H), 7.46 (s, 1H), 7.30 (t, *J* = 7.5 Hz, 2H), 7.23 (t, *J* = 7.5 Hz, 1H), 7.20 – 7.14 (m, 3H), 7.02 (d, *J* = 4.5 Hz, 1H), 4.40 (s, 2H), 3.95 (s, 3H).

Step 3. A solution of 4-benzyl-7-methoxyquinoline (97.4 mg, 0.391 mmol) in anhydrous DCM was cooled to 0 °C under N_2. 1 M solution of tribromoborane in DCM (3.9 mL, 3.9 mmol) was slowly added to the reaction mixture and the reaction mixture was allowed to warm to rt over 2 h. The resulting solution was maintained at ambient temperature for an additional 20 h. The reaction was quenched by addition of ice, and the mixture was diluted with DCM and H_2O. The organic materials were extracted with DCM (100 mL x 3), and washed with saturated $NaHCO_3$ (aq.) followed by dring over Na_2SO_4. The filtered organic layer was concentrated under vacuo. The residue was washed with small portion of DCM (1 mL x 3) and the resulting solid was obtained as the desired product, 4-benzylquinolin-7-ol (beige solid, 74.9 mg, 81%). ^{1}H NMR (300 MHz, methanol-d_4) δ 8.82 (d, *J* = 5.9 Hz, 1H), 8.46 (d, *J* = 9.4 Hz, 1H), 7.55 (d, *J* = 5.9 Hz, 1H), 7.49 (d, *J* = 9.4 Hz, 1H), 7.39 (s, 1H), 7.39 – 7.23 (m, 5H), 4.72 (s, 2H).

Step 4. The mixture of 4-benzylquinolin-7-ol (10.0 mg, 0.0425 mmol), 1,1,1-trifluoro-*N*-phenyl-*N*-((trifluoromethyl)sulfonyl)methanesulfonamide (15.2 mg, 0.0425 mmol) and K_2CO_3 (17.6 mg, 0.128 mmol) in dry THF (0.5 mL) was stirred for 20 min at 120 °C under μW irradtion. The mixture was filtered through a Celite pad and washed with dichloromethane:methanol = 15:1. The filtrate was concentrated under reduced pressure and purified by a flash column chromatography (EtOAc/hexane = 1:10 to 1:4) to give 4-benzylquinolin-7-yl trifluoromethanesulfonate (white solid, 7.8 mg, 50%). ^{1}H NMR (600 MHz, methanol-d_4) δ 8.86 (d, *J* = 4.7 Hz, 1H), 8.36 (d, *J* = 9.4 Hz, 1H), 8.00 (s, 1H), 7.59 (d, *J* = 9.4 Hz, 1H), 7.40 (d, *J* = 4.7 Hz, 1H), 7.35 – 7.27 (m, 2H), 7.27 – 7.19 (m, 3H), 4.54 (s, 2H).

Step 5. Compound **13** (yellow solid, 2.3 mg, 2 steps 46% yield) was prepared by using GP I-2. ^{1}H NMR (400 MHz, methanol-d_4) δ 8.94 (d, *J* = 5.5 Hz, 1H), 8.48 (d, *J* = 8.9 Hz, 1H), 8.44 (s, 1H), 8.31 (s, 1H), 8.18 (d, *J* = 0.7 Hz, 1H), 8.14 (d, *J* = 8.9 Hz, 1H), 7.63 (d, *J* = 5.6 Hz, 1H), 7.39 – 7.22 (m, 5H), 4.72 (s, 2H), 4.66 (tt, *J* = 9.9, 5.2 Hz, 1H), 3.66 – 3.51 (m, 2H), 3.29 – 3.19 (m, 2H), 2.45 – 2.24 (m, 4H). ^{13}C NMR (100 MHz, methanol-d_4) δ 159.6, 146.2, 142.0, 139.8, 138.9, 138.7, 130.2, 130.1, 129.0, 128.7,

128.3, 127.6, 127.4, 122.6, 122.0, 117.4, 57.3, 44.1, 39.4, 30.1. HRMS (ESI$^+$) m/z calcd. $C_{24}H_{25}N_4^+$ [M+H]$^+$: 369.2074, found: 369.2095.

4-phenoxy-7-(1-(piperidin-4-yl)-1*H*-pyrazol-4-yl)quinoline (14). Compound **14** was prepared (15.7 mg, pale yellow solid, 3 steps 46% yield) according to GP II. ^{1}H NMR (400 MHz, methanol-*d*$_4$) δ 8.84 (d, *J* = 6.6 Hz, 1H), 8.63 (d, *J* = 8.8 Hz, 1H), 8.49 (s, 1H), 8.29 (s, 1H), 8.25 − 8.17 (m, 2H), 7.64 (dd, *J* = 8.5, 7.4 Hz, 2H), 7.54 − 7.45 (m, 1H), 7.42 − 7.37 (m, 2H), 6.91 (d, *J* = 6.6 Hz, 1H), 4.68 (tt, *J* = 9.9, 5.1 Hz, 1H), 3.71 − 3.54 (m, 2H), 3.30 − 3.19 (m, 2H), 2.47 − 2.28 (m, 4H). ^{13}C NMR (150 MHz, methanol-*d*$_4$) δ 169.6, 154.2, 147.9, 142.7, 141.2, 139.0, 132.1, 129.2, 128.7, 128.4, 125.1, 122.2, 121.9, 120.4, 115.8, 104.9, 57.3, 44.1, 30.1. HRMS (ESI$^+$) m/z calcd. $C_{23}H_{23}N_4O^+$ [M+H]$^+$: 371.1866, found: 371.1918.

***N*-(2-fluorophenyl)-7-(1-(piperidin-4-yl)-1*H*-pyrazol-4-yl)quinolin-4-amine (15).** Compound **15** was prepared (15.3 mg, white solid, 3 steps 53% yield) according to GP I. ^{1}H NMR (400 MHz, methanol-*d*$_4$) δ 8.56 (d, *J* = 8.8 Hz, 1H), 8.43 (s, 1H), 8.39 (d, *J* = 6.9 Hz, 1H), 8.17 (s, 1H), 8.07 (d, *J* = 9.7 Hz, 2H), 7.62 − 7.49 (m, 2H), 7.46 − 7.36 (m, 2H), 6.59 (d, *J* = 7.0 Hz, 1H), 4.67 (tt, *J* = 10.0, 5.1 Hz, 1H), 3.69 − 3.56 (m, 2H), 3.28 − 3.16 (m, 2H), 2.46 − 2.28 (m, 4H). ^{13}C NMR (100 MHz, methanol-*d*$_4$) δ 159.0 (d, *J* = 249.8 Hz), 157.3, 143.9, 140.8, 140.2, 138.8, 131.5 (d, *J* = 7.9 Hz), 129.8, 128.9, 126.8 (d, *J* = 3.9 Hz), 126.7, 125.9 (d, *J* = 12.7 Hz), 124.8, 121.9, 118.2 (d, *J* = 19.8 Hz), 116.8, 115.6, 101.4, 57.3, 44.1, 30.2. ^{19}F NMR (376 MHz, methanol-*d*$_4$) δ -76.9, -122.1. HRMS (ESI$^+$) m/z calcd. $C_{23}H_{23}FN_5^+$ [M+H]$^+$: 388.1932, found: 388.1916.

4-(2-fluorophenoxy)-7-(1-(piperidin-4-yl)-1*H*-pyrazol-4-yl)quinoline (16). Compound **16** was prepared (11.2 mg, white solid, 3 steps 29% yield) according to GP II. ^{1}H NMR (400 MHz, methanol-*d*$_4$) δ 8.83 (d, *J* = 6.2 Hz, 1H), 8.58 (d, *J* = 8.8 Hz, 1H), 8.46 (s, 1H), 8.27 (s, 1H), 8.20 (s, 1H), 8.16 (d, *J* = 8.8 Hz, 1H), 7.56 − 7.36 (m, 4H), 6.87 (d, *J* = 6.2 Hz, 1H), 4.67 (dq, *J* = 9.9, 5.2 Hz, 1H), 3.71 − 3.54 (m, 2H), 3.30 − 3.17 (m, 2H), 2.57 − 2.23 (m, 4H). ^{13}C NMR (150 MHz, methanol-*d*$_4$) δ 167.7, 155.3 (d, *J* = 249.4 Hz), 148.8, 144.0, 141.2 (d, *J* = 12.4 Hz), 140.6, 139.0, 130.1 (d, *J* = 6.9 Hz), 129.1, 128.3, 127.3 (d, *J* = 3.8 Hz), 124.7 (d, *J* = 2.9 Hz), 122.1, 120.0, 118.9 (d, *J* = 17.8 Hz), 117.1, 111.4, 104.5, 57.3, 44.1,

30.2. ^{19}F NMR (376 MHz, methanol-d_4) δ -76.9, -131.7. HRMS (ESI$^+$) m/z calcd. $C_{23}H_{22}FN_4O^+$ [M+H]$^+$: 389.1772, found: 389.1781.

N-(3-fluorophenyl)-7-(1-(piperidin-4-yl)-1H-pyrazol-4-yl)quinolin-4-amine (17). Compound **17** was prepared (9.3 mg, pale yellow solid, 3 steps 48% yield) according to GP I. ^{1}H NMR (400 MHz, methanol-d_4) δ 8.54 (d, J = 9.2 Hz, 1H), 8.44 (s, 1H), 8.39 (d, J = 7.0 Hz, 1H), 8.17 (s, 1H), 8.10 − 8.01 (m, 2H), 7.60 (td, J = 8.2, 6.4 Hz, 1H), 7.38 − 7.28 (m, 2H), 7.21 (td, J = 8.2, 2.4 Hz, 1H), 6.95 (d, J = 7.0 Hz, 1H), 4.67 (tt, J = 9.9, 5.2 Hz, 1H), 3.71 − 3.53 (m, 2H), 3.29 − 3.20 (m, 2H), 2.54 − 2.22 (m, 4H). ^{13}C NMR (150 MHz, methanol-d_4) δ 164.9 (d, J = 246.8 Hz), 156.6, 144.1, 141.2, 140.4 (d, J = 9.8 Hz), 140.1, 138.8, 132.8 (d, J = 9.2 Hz), 128.8, 126.6, 124.8, 122.3 (d, J = 3.0 Hz), 121.9, 117.2, 115.8, 115.6 (d, J = 21.3 Hz), 113.7 (d, J = 24.0 Hz), 101.3, 57.3, 44.1, 30.2. ^{19}F NMR (376 MHz, methanol-d_4) δ -76.9, -112.4. HRMS (ESI$^+$) m/z calcd. $C_{23}H_{23}FN_5^+$ [M+H]$^+$: 388.1932, found: 388.1990.

4-(3-fluorophenoxy)-7-(1-(piperidin-4-yl)-1H-pyrazol-4-yl)quinoline (18). Compound **18** was prepared (4.8 mg, white solid, 3 steps 53% yield) according to GP II. ^{1}H NMR (400 MHz, methanol-d_4) δ 8.86 (d, J = 6.5 Hz, 1H), 8.60 (d, J = 8.8 Hz, 1H), 8.48 (s, 1H), 8.28 (s, 1H), 8.24 − 8.16 (m, 2H), 7.71 − 7.58 (m, 1H), 7.31 − 7.19 (m, 3H), 6.98 (d, J = 6.5 Hz, 1H), 4.68 (tt, J = 9.9, 4.9 Hz, 1H), 3.70 − 3.51 (m, 2H), 3.29 − 3.20 (m, 2H), 2.47 − 2.25 (m, 4H). ^{13}C NMR (150 MHz, methanol-d_4) δ 167.2, 165.1 (d, J = 248.4 Hz), 155.5 (d, J = 11.0 Hz), 149.4, 145.2, 139.8, 138.8, 133.2 (d, J = 9.5 Hz), 128.8, 127.8, 124.6, 122.3, 120.6, 118.2, 118.2, 115.1 (d, J = 21.2 Hz), 110.2 (d, J = 24.9 Hz), 105.2, 57.3, 44.1, 30.2. ^{19}F NMR (376 MHz, methanol-d_4) δ -76.7, -110.7. HRMS (ESI$^+$) m/z calcd. $C_{23}H_{22}FN_4O^+$ [M+H]$^+$: 389.1772, found: 389.1782.

N-(4-fluorophenyl)-7-(1-(piperidin-4-yl)-1H-pyrazol-4-yl)quinolin-4-amine (19). Compound **19** was prepared (11.6 mg, pale yellow solid, 3 steps 70% yield) according to GP I. ^{1}H NMR (400 MHz, methanol-d_4) δ 8.53 (d, J = 9.4 Hz, 1H), 8.43 (s, 1H), 8.34 (d, J = 7.1 Hz, 1H), 8.16 (s, 1H), 8.10 − 8.02 (m, 2H), 7.55 − 7.45 (m, 2H), 7.33 (t, J = 8.6 Hz, 2H), 6.76 (d, J = 7.0 Hz, 1H), 4.67 (dq, J = 9.8, 4.8 Hz, 1H), 3.67 − 3.53 (m, 2H), 3.29 − 3.22 (m, 2H), 2.50 − 2.23 (m, 4H). ^{13}C NMR (100 MHz, methanol-d_4) δ 163.3 (d,

J = 246.6 Hz), 157.3, 143.6, 140.8, 140.2, 138.8, 134.6, 129.1 (d, J = 8.7 Hz), 128.9, 126.6, 124.8, 121.9, 118.0 (d, J = 23.2 Hz), 116.8, 115.5, 100.8, 57.3, 44.1, 30.2. ^{19}F NMR (376 MHz, methanol-d_4) δ -76.9, -115.3. HRMS (ESI$^+$) m/z calcd. $C_{23}H_{23}FN_5^+$ [M+H]$^+$: 388.1932, found: 388.1945.

4-(4-fluorophenoxy)-7-(1-(piperidin-4-yl)-1H-pyrazol-4-yl)quinoline (20). Compound **20** was prepared (8.3 mg, white solid, 3 steps 27% yield) according to GP II. ^{1}H NMR (400 MHz, methanol-d_4) δ 8.86 (d, J = 6.4 Hz, 1H), 8.61 (d, J = 8.8 Hz, 1H), 8.49 (d, J = 2.3 Hz, 1H), 8.29 (s, 1H), 8.24 – 8.12 (m, 2H), 7.48 – 7.39 (m, 2H), 7.40 – 7.29 (m, 2H), 6.93 (d, J = 6.5 Hz, 1H), 4.68 (tt, J = 10.1, 5.1 Hz, 1H), 3.74 – 3.54 (m, 2H), 3.28 – 3.21 (m, 2H), 2.48 – 2.25 (m, 4H). ^{13}C NMR (100 MHz, methanol-d_4) δ 169.3, 162.6 (d, J = 245.3 Hz), 150.2, 148.2, 143.0, 141.0, 139.0, 129.1, 128.4, 125.0, 124.2 (d, J = 8.8 Hz), 121.9, 120.4, 118.7 (d, J = 24.2 Hz), 116.2, 104.8, 57.3, 44.2, 30.1. ^{19}F NMR (376 MHz, methanol-d_4) δ -76.9, -116.6. HRMS (ESI$^+$) m/z calcd. $C_{23}H_{22}FN_4O^+$ [M+H]$^+$: 389.1772, found: 389.1786.

N-(3,4-difluorophenyl)-7-(1-(piperidin-4-yl)-1H-pyrazol-4-yl)quinolin-4-amine (21). Compound **21** was prepared (14.7 mg, yellow solid, 3 steps 63% yield) according to GP I. ^{1}H NMR (400 MHz, methanol-d_4) δ 8.51 (d, J = 8.9 Hz, 1H), 8.43 (s, 1H), 8.39 (d, J = 7.0 Hz, 1H), 8.17 (s, 1H), 8.06 (d, J = 8.1 Hz, 2H), 7.55 – 7.42 (m, 2H), 7.37 – 7.27 (m, 1H), 6.88 (d, J = 6.9 Hz, 1H), 4.67 (tt, J = 10.0, 5.1 Hz, 1H), 3.72 – 3.56 (m, 2H), 3.29 – 3.18 (m, 2H), 2.48 – 2.23 (m, 4H). ^{13}C NMR (100 MHz, methanol-d_4) δ 157.0, 152.1 (dd, J = 249.5, 13.8 Hz), 150.9 (dd, J = 248.1, 12.6 Hz), 144.0, 140.9, 140.2, 138.8, 135.3 (d, J = 3.6 Hz), 128.9, 126.7, 124.8, 123.7 (dd, J = 6.6, 3.5 Hz), 121.8, 119.8 (d, J = 18.6 Hz), 117.0, 116.5 (d, J = 19.4 Hz), 115.6, 101.1, 57.3, 44.1, 30.2. ^{19}F NMR (376 MHz, methanol-d_4) δ -76.9, -136.8 (d, J = 20.8 Hz), -140.5 (d, J = 20.8 Hz). HRMS (ESI$^+$) m/z calcd. $C_{23}H_{22}F_2N_5^+$ [M+H]$^+$: 406.1838, found: 406.1840.

4-(3,4-difluorophenoxy)-7-(1-(piperidin-4-yl)-1H-pyrazol-4-yl)quinoline (22). Compound **22** was prepared (0.6 mg, pale yellow solid, 3 steps 28% yield) according to GP II. ^{1}H NMR (400 MHz, methanol-d_4) δ 8.89 (d, J = 6.6 Hz, 1H), 8.59 (d, J = 8.8 Hz, 1H), 8.49 (s, 1H), 8.31 (s, 1H), 8.26 – 8.18 (m, 2H), 7.61 – 7.45 (m, 2H), 7.27 (dtd, J = 9.1, 3.2, 1.6 Hz, 1H), 7.03 (d, J = 6.6 Hz, 1H), 4.68 (tt, J = 9.9, 5.1 Hz, 1H), 3.68 – 3.55 (m, 2H), 3.30 – 3.20 (m, 2H), 2.52 – 2.24 (m, 4H). ^{13}C NMR (100 MHz, methanol-d_4) δ

169.1, 152.3 (dd, $J = 251.1, 14.3$ Hz), 150.6 (dd, $J = 247.3, 12.4$ Hz), 149.8 (dd, $J = 8.6, 3.2$ Hz), 148.0,

142.7, 141.3, 139.0, 129.2, 128.6, 124.0, 121.8, 120.3, 120.1 (d, $J = 19.5$ Hz), 119.2 (dd, $J = 6.7, 3.9$ Hz),

115.8, 112.72 (d, $J = 20.5$ Hz), 105.0, 57.3, 44.1, 30.1. ^{19}F NMR (376 MHz, methanol-d_4) δ -77.0, -135.8

(d, $J = 20.6$ Hz), -143.0 (d, $J = 20.8$ Hz). HRMS (ESI[+]) m/z calcd. $C_{23}H_{21}F_2N_4O^+$ [M+H][+]: 407.1678,

found: 407.1697.

7-(1-(piperidin-4-yl)-1*H*-pyrazol-4-yl)-*N*-(p-tolyl)quinolin-4-amine (23). Compound **23** was prepared

(14.7 mg, pale brown solid, 3 steps 67% yield) according to GP I. ^{1}H NMR (400 MHz, methanol-d_4) δ

8.52 (d, $J = 9.1$ Hz, 1H), 8.42 (s, 1H), 8.30 (d, $J = 7.1$ Hz, 1H), 8.15 (s, 1H), 8.07 − 7.98 (m, 2H), 7.40 (d,

$J = 8.1$ Hz, 2H), 7.34 (d, $J = 8.1$ Hz, 2H), 6.78 (d, $J = 7.1$ Hz, 1H), 4.66 (dq, $J = 10.2, 5.5$ Hz, 1H), 3.68

− 3.55 (m, 2H), 3.28 − 3.17 (m, 2H), 2.43 (s, 3H), 2.41 − 2.27 (m, 4H). ^{13}C NMR (150 MHz, methanol-

d_4) δ 157.2, 143.4, 140.8, 140.0, 139.4, 138.7, 135.8, 131.8, 128.8, 126.6, 126.4, 124.8, 121.9, 116.9,

115.6, 100.8, 57.3, 44.1, 30.2, 21.1. HRMS (ESI[+]) m/z calcd. $C_{24}H_{26}N_5^+$ [M+H][+]: 384.2183, found:

384.2186.

7-(1-(piperidin-4-yl)-1*H*-pyrazol-4-yl)-4-(*p*-tolyloxy)quinoline (24) Compound **24** was prepared (15.7

mg, pale yellow solid, 3 steps 53% yield) according to GP II. ^{1}H NMR (600 MHz, methanol-d_4) δ 8.83

(d, $J = 6.4$ Hz, 1H), 8.60 (d, $J = 8.8$ Hz, 1H), 8.48 (s, 1H), 8.28 (s, 1H), 8.20 (d, $J = 9.8$ Hz, 2H), 7.43 (d,

$J = 8.0$ Hz, 2H), 7.25 (d, $J = 8.0$ Hz, 2H), 6.90 (d, $J = 6.4$ Hz, 1H), 4.68 (tt, $J = 9.8, 4.5$ Hz, 1H), 3.68 −

3.58 (m, 2H), 3.30 − 3.22 (m, 2H), 2.45 (s, 3H), 2.44 − 2.28 (m, 4H). ^{13}C NMR (150 MHz, methanol-d_4)

δ 169.7, 152.0, 147.9, 142.8, 141.1, 139.0, 138.8, 132.5, 129.1, 128.3, 125.1, 121.9, 121.8, 120.4, 115.9,

104.8, 57.3, 44.1, 30.1, 21.0. HRMS (ESI[+]) m/z calcd. $C_{24}H_{25}N_4O^+$ [M+H][+]: 385.2023, found: 385.2028.

4-((7-(1-(piperidin-4-yl)-1*H*-pyrazol-4-yl)quinolin-4-yl)amino)benzonitrile (25). Compound **25** was

prepared (3.3 mg, pale yellow solid, 3 steps 49% yield) according to GP I. ^{1}H NMR (400 MHz, methanol-

d_4) δ 8.55 (d, $J = 8.9$ Hz, 1H), 8.45 (d, $J = 7.0$ Hz, 1H), 8.44 (s, 1H), 8.15 (s, 1H), 8.09 (s, 1H), 8.07 (d, J

$= 8.9$ Hz, 1H), 7.91 (d, $J = 8.5$ Hz, 2H), 7.68 (d, $J = 8.5$ Hz, 2H), 7.11 (d, $J = 6.9$ Hz, 1H), 4.67 (tt, $J =$

10.0, 5.3 Hz, 1H), 3.71 − 3.47 (m, 2H), 3.30 − 3.17 (m, 2H), 2.47 − 2.24 (m, 4H). ^{13}C NMR (100 MHz,

methanol-d_4) δ 156.0, 144.1, 143.2, 140.9, 140.4, 138.8, 135.2, 128.9, 127.0, 126.3, 124.9, 121.7, 119.2, 117.6, 115.5, 111.5, 101.8, 57.3, 44.1, 30.1. HRMS (ESI$^+$) m/z calcd. $C_{24}H_{23}N_6^+$ [M+H]$^+$: 395.1979, found: 395.2017.

4-((7-(1-(piperidin-4-yl)-1*H*-pyrazol-4-yl)quinolin-4-yl)oxy)benzonitrile (26). Compound **26** was prepared (8.6 mg, white solid, 3 stesp 46% yield) according to GP II. ^{1}H NMR (400 MHz, methanol-d_4) δ 8.83 (d, *J* = 6.0 Hz, 1H), 8.49 (d, *J* = 8.8 Hz, 1H), 8.43 (s, 1H), 8.26 (s, 1H), 8.18 (s, 1H), 8.11 (d, *J* = 8.8 Hz, 1H), 7.97 (d, *J* = 8.9 Hz, 2H), 7.54 (d, *J* = 8.7 Hz, 2H), 6.95 (d, *J* = 6.0 Hz, 1H), 4.67 (tt, *J* = 9.9, 4.8 Hz, 1H), 3.70 – 3.55 (m, 2H), 3.30 – 3.22 (m, 2H), 2.52 – 2.28 (m, 4H). ^{13}C NMR (100 MHz, methanol-d_4) δ 166.3, 158.2, 149.6, 145.5, 139.9, 138.9, 136.3, 128.9, 128.0, 124.5, 123.2, 122.2, 120.8, 118.9, 118.4, 111.8, 106.0, 57.3, 44.1, 30.2. HRMS (ESI$^+$) m/z calcd. $C_{24}H_{22}N_5O^+$ [M+H]$^+$: 396.1819, found: 396.1828.

***N*-(4-methoxyphenyl)-7-(1-(piperidin-4-yl)-1*H*-pyrazol-4-yl)quinolin-4-amine (27).** Compound **27** was prepared (13.2 mg, yellow solid, 3 steps 45% yield) according to GP I. ^{1}H NMR (400 MHz, methanol-d_4) δ 8.51 (d, *J* = 9.3 Hz, 1H), 8.42 (s, 1H), 8.28 (d, *J* = 7.1 Hz, 1H), 8.15 (s, 1H), 8.06 – 7.98 (m, 2H), 7.38 (d, *J* = 8.8 Hz, 2H), 7.12 (d, *J* = 8.8 Hz, 2H), 6.71 (d, *J* = 7.1 Hz, 1H), 4.66 (tt, *J* = 10.0, 5.4 Hz, 1H), 3.87 (s, 3H), 3.67 – 3.55 (m, 2H), 3.29 – 3.19 (m, 2H), 2.47 – 2.25 (m, 4H). ^{13}C NMR (150 MHz, methanol-d_4) δ 160.9, 157.5, 143.3, 140.7, 140.0, 138.7, 130.8, 128.8, 128.3, 126.4, 124.8, 121.9, 116.7, 116.4, 115.5, 100.7, 57.3, 56.1, 44.1, 30.2. HRMS (ESI$^+$) m/z calcd. $C_{24}H_{26}N_5O^+$ [M+H]$^+$: 400.2132, found: 400.2132.

4-(4-methoxyphenoxy)-7-(1-(piperidin-4-yl)-1*H*-pyrazol-4-yl)quinoline (28). Compound **28** was prepared (8.5 mg, white solid, 3 steps 37% yield) according to GP II. ^{1}H NMR (400 MHz, methanol-d_4) δ 8.77 (d, *J* = 6.3 Hz, 1H), 8.57 (d, *J* = 8.8 Hz, 1H), 8.44 (s, 1H), 8.22 (s, 1H), 8.19 (s, 1H), 8.13 (d, *J* = 8.8 Hz, 1H), 7.27 (d, *J* = 9.1 Hz, 2H), 7.13 (d, *J* = 9.1 Hz, 2H), 6.82 (d, *J* = 6.3 Hz, 1H), 4.67 (tt, *J* = 9.9, 4.8 Hz, 1H), 3.88 (s, 3H), 3.66 – 3.55 (m, 2H), 3.29 – 3.20 (m, 2H), 2.49 – 2.28 (m, 4H). ^{13}C NMR (100 MHz, methanol-d_4) δ 167.6, 159.7, 150.1, 147.9, 139.0, 138.8, 128.6, 127.2, 127.2, 124.5, 123.2, 122.6,

120.7, 119.3, 116.7, 104.6, 57.2, 56.2, 44.1, 30.2. HRMS (ESI$^+$) m/z calcd. $C_{24}H_{25}N_4O_2^+$ [M+H]$^+$: 401.1972, found: 401.1966.

4-((7-(1-(piperidin-4-yl)-1*H*-pyrazol-4-yl)quinolin-4-yl)amino)phenol (29). Compound **29** was prepared (16.1 mg, yellow solid, 3 steps 66% yield) according to GP I. ^{1}H NMR (600 MHz, methanol-d_4) δ 8.49 (d, *J* = 9.2 Hz, 1H), 8.41 (s, 1H), 8.26 (d, *J* = 7.1 Hz, 1H), 8.14 (s, 1H), 8.02 – 7.97 (m, 2H), 7.26 (d, *J* = 8.7 Hz, 2H), 6.96 (d, *J* = 8.7 Hz, 2H), 6.69 (d, *J* = 7.1 Hz, 1H), 4.66 (tt, *J* = 9.9, 4.8 Hz, 1H), 3.66 – 3.56 (m, 2H), 3.30 – 3.20 (m, 2H), 2.45 – 2.29 (m, 4H). ^{13}C NMR (150 MHz, methanol-d_4) δ 158.8, 157.6, 143.1, 140.6, 140.0, 138.7, 129.6, 128.8, 128.4, 126.3, 124.8, 121.9, 117.7, 116.6, 115.4, 100.7, 57.3, 44.1, 30.2. HRMS (ESI$^+$) m/z calcd. $C_{23}H_{24}N_5O^+$ [M+H]$^+$: 386.1975, found: 386.1954.

4-((7-(1-(piperidin-4-yl)-1*H*-pyrazol-4-yl)quinolin-4-yl)oxy)phenol (30). Compound **30** was prepared (4.8 mg, white solid, 3 steps 37% yield) according to GP II. ^{1}H NMR (400 MHz, methanol-d_4) δ 8.80 (d, *J* = 6.5 Hz, 1H), 8.59 (d, *J* = 8.8 Hz, 1H), 8.46 (s, 1H), 8.25 (s, 1H), 8.20 (s, 1H), 8.17 (d, *J* = 8.9 Hz, 1H), 7.17 (d, *J* = 8.9 Hz, 2H), 6.97 (d, *J* = 8.9 Hz, 2H), 6.90 (d, *J* = 6.5 Hz, 1H), 4.67 (tt, *J* = 9.9, 5.0 Hz, 1H), 3.69 – 3.51 (m, 2H), 3.30 – 3.21 (m, 2H), 2.46 – 2.27 (m, 4H). ^{13}C NMR (150 MHz, methanol-d_4) δ 168.8, 157.6, 149.1, 146.8, 144.8, 139.8, 138.8, 128.8, 127.6, 124.7, 123.1, 122.3, 120.5, 118.0, 117.9, 104.6, 57.2, 44.1, 30.2. HRMS (ESI$^+$) m/z calcd. $C_{23}H_{23}N_4O_2^+$ [M+H]$^+$: 387.1816, found: 387.1806.

Enzymatic assay. The inhibitory activities of all compounds with respect to ALK and ALK (L1196M) were measured by Reaction Biology Corp. (Malvern, PA, USA) by means of radiometric kinase assays ([γ-^{33}P]ATP). The enzymatic activity of ALK and ALK (L1196M) was monitored using 20 μM of peptide substrate, [YRRAAVPPSPSLSRHSSPHQ(pS)EDEEE] dissolved in the freshly prepared Reaction Buffer (20 mM HEPES (pH 7.5), 10 mM MgCl$_2$, 1 mM EGTA, 0.02% BRIJ-35, 0.02 mg/mL BSA, 0.1 mM Na$_3$VO$_4$, 2 mM DTT, 1% DMSO). Each putative ALK and ALK (L1196M) inhibitor was dissolved in 100% DMSO at the specific concentration and diluted in serial manner with epMotion 5070 in DMSO. Four nM of ALK and ALK (L1196M) (Invitrogen) was added into the reaction buffer including 20 μM

of peptide substrate. After delivering the candidate inhibitor dissolved in DMSO into the kinase reaction mixture by Acoustic technology (Echo550; nanoliter range), the reaction mixture was incubated for 20 min at room temperature. To initiate the enzymatic reaction, ^{33}P-ATP with specific activity of 10 μCi/μL was delivered into the reaction mixture to reach the final ATP concentration of 10 μM. Radioactivity was then monitored by the filterbinding method after the incubation of reaction mixture for 2 h at room temperature. At given concentrations of the inhibitor, biochemical potency was measured by the percent remaining kinase activity with respect to vehicle (dimethyl sulfoxide) reaction. Curve fits and IC_{50} values were then obtained using the PRISM program (GraphPad Software). The ATP-competitive inhibitor staurosporine (STSP) was employed as the positive control in this study because of its high biochemical potency against various kinases including ALK and ALK (L1196M). Kinase panel assays were carried out at Ambit Bioscience Corp. (San Diego, CA, USA) using the potent and broad-spectrum kinase inhibitor (staurosporine) as the reference.

Cells and meterials. H2228 human lung cancer cells were purchased from the American Type Culture Collection (ATCC Manassas, VA). H2228 cells were cultured in RPMI 1640 medium supplemented with 10% FBS and 1% penicillin/ streptomycin. Crizotinib resistant subline, H2228 CR cells were cultured in RPMI 1640 medium supplemented with 10% FBS, 1% penicillin/ streptomycin and 100 nM crizotinib. Cell culture media, FBS, penicillin-streptomycin, and other supplementary agents were purchased from GIBCO (Uxbridge, UK). 3-(4,5-dimethylthiazol-2-yl)-2,5-diphenyltetrazolium bromide (MTT) was purchased from Sigma-Aldrich (St. Louis, MO). All cell lines were maintained in a CO_2 incubator with a controlled humidified atmosphere composed of 95% air and 5% CO_2. Crizotinib was purchased from LC laboratories (Woburn, MA) and dissolved in DMSO.

Generation of crizotinib-resistant cells. Crizotinib-resistant cells were generated as previously reported. In brief, H2228 CR cells were developed by chronic, repeated exposure to crizotinib. Over a period of 8 months, H2228 cells were continuously exposed to increasing concentrations of the drug in culture and

the surviving cells were cloned. These cells could survive exposure >100 nM of crizotinib. In all studies, resistant cells were cultured in drug-free medium for >1 week to eliminate the effects of crizotinib.

Cell growth assay. H2228 and H2228 CR were plated at a density of 4,000 cells/well in 96 well plates and incubated for 24 h. The medium was then removed, and cells were treated with different concentrations of crizotinib and **30** for 72 h. Next, 20 μL of MTT solution (2 mg/mL) was added for 4 h at 37 ºC in 5% CO_2 incubator. After the media was then removed, 200 μL of DMSO was added to each well, and the plate was incubated for an additional 4 h at 37°C. The formazan crystals that formed in metabolically healthy cells were dissolved in DMSO (200 µL/well) with constant shaking for 30 min. Absorbance of the solution was then measured with a microplate reader at 540 nm.

Western blotting. H2228 and H2228CR were seeded in 10 cm plate dish and incubated overnight for attachment. Crizotinib and **30** were treated for 3 h in serum-free medium. Total cellular proteins were extracted with sterile RIPA lysis buffer (Biosesang, Korea) consisting of 150 mmol/L NaCl, 1% Triton X-100, 1% sodium deoxycholate, 0.1% SDS, 50 mmol/L Tris-HCl pH 7.5, and 2 mmol/L EDTA supplemented with Xpert Protease & Phosphatase Inhibitor cocktail (GenDEPOT, Barker, TX) solution (100X) prior to use. The proteins were separated by sodium dodecyl sulfate-polyacrylamide gel electrophoresis (SDS-PAGE) and transferred onto nitrocellulose membranes. Membranes were incubated first with diluted primary antibodies overnight with gentle shaking at 4°C, and then with horseradish peroxidase (HRP)-conjugated secondary antibodies. Thereafter, membranes were washed in PBS containing 0.1% Tween-20 (PBST), and were visualized using enhanced chemiluminescence reagents (Clarity Western ECL Substrate; Bio-Rad, Hercules, CA). Antibodies against p-AKT, AKT, p-ERK, ERK, and β-actin were purchased from Cell Signaling Technology (Danvers, MA) and Sigma-Aldrich.

ASSOCIATED CONTENTS

Supporting information: The Supporting Information is available free of charge via the Internet at http://pubs.acs.org.

Spectral data for all listed compounds (PDF)

Molecular formula strings (CSV)

Atomic coordinates of computational models (MOL)

AUTHOR INFORMATION

Corresponding Author

*For S.H.: phone, (+82) 42 3502811; E-mail: hongorg@kaist.ac.kr.

*For FS.S.H.: phone, (+82) 32-890-3683; E-mail: hongs@inha.ac.kr.

[+] These authors contributed equally to this work

ABBREVIATIONS USED

ALK, anaplastic lymphoma kinase; WT, wild type; NSCLC, non-small cell lung cancer; EML4, echinoderm microtubule-associated protein-like 4; RTK, receptor tyrosine kinase; MK, midkine; PTN, pleiotrophin; PI3K, phosphatidylinositol-4,5-bisphosphate 3-kinase; AKT, protein kinase B; JAK, janus kinase; STAT, signal transducer and activator of transcription protein; MEK, mitogen-activated protein kinase kinase; ERK, extracellular signal-regulated kinases; MAPK, mitogen-activated protein kinases; c-Met, tyrosine-protein kinase Met; CR, crizotinib-resistant; PDB, protein data bank; SAR, structure-activity relationship; S_NAr, nucleophilic aromatic substitution; MTT, 3-(4,5-dimethylthiazol-2-yl)-2,5-diphenyltetrazolium bromide; POC, percent of control; ATP, adenosine triphosphate; HEPES, 4-(2-hydroxyethyl)-1-piperazineethanesulfonic acid; hERG, human ether-a-go-go-related gene K^+ channel.

REFERENCES

1. Motegi, A.; Fujimoto, J.; Kotani, M.; Sakuraba, H.; Yamamoto, T. ALK receptor tyrosine kinase promotes cell growth and neurite outgrowth. *J. Cell Sci.* **2004,** *117,* 3319−3329.

2. García-Regalado, A.; González-De la Rosa, C. H. The role of anaplastic lymphoma kinase in human cancers. *Oncology & Hematology Review* **2013,** *9,* 149−153.

3. Hallberg, B.; Palmer, R. H. Mechanistic insight into ALK receptor tyrosine kinase in human cancer biology. *Nat. Rev. Cancer* **2013,** *13,* 685−700.

4. Roskoski, R. Anaplastic lymphoma kinase (ALK): structure, oncogenic activation, and pharmacological inhibition. *Pharmacol. Res.* **2013,** *68,* 68−94.

5. Koivunen, J. P.; Mermel, C.; Zejnullahu, K.; Murphy, C.; Lifshits, E.; Holmes, A. J.; Choi, H. G.; Kim, J.; Chiang, D.; Thomas, R. EML4-ALK fusion gene and efficacy of an ALK kinase inhibitor in lung cancer. *Clin. Cancer Res.* **2008,** *14,* 4275−4283.

6. Palmer, R. H.; Vernersson, E.; Grabbe, C.; Hallberg, B. Anaplastic lymphoma kinase: signalling in development and disease. *Biochem. J.* **2009,** *420,* 345−361.

7. Soda, M.; Choi, Y. L.; Enomoto, M.; Takada, S.; Yamashita, Y.; Ishikawa, S.; Fujiwara, S.-i.; Watanabe, H.; Kurashina, K.; Hatanaka, H. Identification of the transforming EML4−ALK fusion gene in non-small-cell lung cancer. *Nature* **2007,** *448,* 561−566.

8. Friboulet, L.; Li, N.; Katayama, R.; Lee, C. C.; Gainor, J. F.; Crystal, A. S.; Michellys, P.-Y.; Awad, M. M.; Yanagitani, N.; Kim, S. The ALK inhibitor ceritinib overcomes crizotinib resistance in non−small cell lung cancer. *Cancer Discov.* **2014,** *4,* 662−673.

9. Sakamoto, H.; Tsukaguchi, T.; Hiroshima, S.; Kodama, T.; Kobayashi, T.; Fukami, T. A.; Oikawa, N.; Tsukuda, T.; Ishii, N.; Aoki, Y. CH5424802, a selective ALK inhibitor capable of blocking the resistant gatekeeper mutant. *Cancer cell* **2011,** *19,* 679−690.

10. Mori, M.; Ueno, Y.; Konagai, S.; Fushiki, H.; Shimada, I.; Kondoh, Y.; Saito, R.; Mori, K.; Shindou, N.; Soga, T. The selective anaplastic lymphoma receptor tyrosine kinase inhibitor ASP3026 induces tumor regression and prolongs survival in non−small cell lung cancer model mice. *Mol. Cancer Ther.* **2014,** *13,* 329−340.

11. Ott, G. R.; Cheng, M.; Learn, K. S.; Wagner, J.; Gingrich, D. E.; Lisko, J. G.; Curry, M.; Mesaros, E. F.; Ghose, A. K.; Quail, M. R. Discovery of clinical candidate CEP-37440, a selective inhibitor of focal adhesion kinase (FAK) and anaplastic lymphoma kinase (ALK). *J. Med. Chem.* **2016,** *59*, 7478−7496.

12. Cui, J. J.; Tran-Dubé, M.; Shen, H.; Nambu, M.; Kung, P.-P.; Pairish, M.; Jia, L.; Meng, J.; Funk, L.; Botrous, I. Structure based drug design of crizotinib (PF-02341066), a potent and selective dual inhibitor of mesenchymal–epithelial transition factor (c-MET) kinase and anaplastic lymphoma kinase (ALK). *J. Med. Chem.* **2011,** *54*, 6342−6363.

13. Zhang, S.; Anjum, R.; Squillace, R.; Nadworny, S.; Zhou, T.; Keats, J.; Ning, Y.; Wardwell, S. D.; Miller, D.; Song, Y. The potent ALK inhibitor brigatinib (AP26113) overcomes mechanisms of resistance to first-and second-generation ALK inhibitors in preclinical models. *Clin. Cancer Res.* **2016,** *22*, 5527−5538.

14. Iwama, E.; Okamoto, I.; Harada, T.; Takayama, K.; Nakanishi, Y. Development of anaplastic lymphoma kinase (ALK) inhibitors and molecular diagnosis in ALK rearrangement-positive lung cancer. *Onco Targets Ther.* **2014,** *7*, 375−385.

15. Katayama, R.; Shaw, A. T.; Khan, T. M.; Mino-Kenudson, M.; Solomon, B. J.; Halmos, B.; Jessop, N. A.; Wain, J. C.; Yeo, A. T.; Benes, C. Mechanisms of acquired crizotinib resistance in ALK-rearranged lung cancers. *Sci. Transl. Med.* **2012,** *4*, No. 120ra17.

16. Fontana, D.; Ceccon, M.; Gambacorti-Passerini, C.; Mologni, L. Activity of second-generation ALK inhibitors against crizotinib-resistant mutants in an NPM-ALK model compared to EML4-ALK. *Cancer Med.* **2015,** *4*, 953−965.

17. Lin, Y.-T.; Yu, C.-J.; Yang, J. C.-H.; Shih, J.-Y. Anaplastic lymphoma kinase (ALK) kinase domain mutation following ALK Inhibitor (s) failure in advanced ALK positive non–small-cell lung cancer: analysis and literature review. *Clin. lung cancer* **2016,** *17*, e77-e94.

18. Toyokawa, G.; Inamasu, E.; Shimamatsu, S.; Yoshida, T.; Nosaki, K.; Hirai, F.; Yamaguchi, M.; Seto, T.; Takenoyama, M.; Ichinose, Y. Identification of a novel ALK G1123S mutation in a patient with ALK-

rearranged non–small-cell lung cancer exhibiting resistance to ceritinib. *J. Thorac. Oncol.* **2015,** 10, e55-e57.

19. Ou, S.-H. I.; Azada, M.; Hsiang, D. J.; Herman, J. M.; Kain, T. S.; Siwak-Tapp, C.; Casey, C.; He, J.; Ali, S. M.; Klempner, S. J. Next-generation sequencing reveals a Novel NSCLC ALK F1174V mutation and confirms ALK G1202R mutation confers high-level resistance to alectinib (CH5424802/RO5424802) in ALK-rearranged NSCLC patients who progressed on crizotinib. *J. Thorac. Oncol.* **2014,** *9*, 549−553.

20. Gadgeel, S. M.; Gandhi, L.; Riely, G. J.; Chiappori, A. A.; West, H. L.; Azada, M. C.; Morcos, P. N.; Lee, R.-M.; Garcia, L.; Yu, L. Safety and activity of alectinib against systemic disease and brain metasta ses in patients with crizotinib-resistant ALK-rearranged non-small-cell lung cancer (AF-002JG): results from the dose-finding portion of a phase 1/2 study. *Lancet Oncol.* **2014**, *15*, 1119−1128.

21. Katayama, R.; Lovly, C. M.; Shaw, A. T. Therapeutic targeting of anaplastic lymphoma kinase in lung cancer: a paradigm for precision cancer medicine. *Clin. Cancer Res.* **2015**, *21*, 2227−2235.

22. Zhang, J.; Yang, P. L.; Gray, N. S. Targeting cancer with small molecule kinase inhibitors. *Nat. Rev. Cancer* **2009,** *9*, 28−39.

23. Li, J.; Liu, W.; Luo, H.; Bao, J. Insight into drug resistance mechanisms and discovery of potential inhibitors against wild-type and L1196M mutant ALK from FDA-approved drugs. *J. Mol. Model.* **2016,** *22*, 231.

24. Ai, X.; Shen, S.; Shen, L.; Lu, S. An interaction map of small-molecule kinase inhibitors with anaplastic lymphoma kinase (ALK) mutants in ALK-positive non-small cell lung cancer. *Biochimie* **2015,** *112*, 111−120.

25. BiochimieBossi, R. T.; Saccardo, M. B.; Ardini, E.; Menichincheri, M.; Rusconi, L.; Magnaghi, P.; Orsini, P.; Avanzi, N.; Borgia, A. L.; Nesi, M. Crystal structures of anaplastic lymphoma kinase in complex with ATP competitive inhibitors. *Biochemistry* **2010,** *49*, 6813−6825.

26. Huang, Q.; Johnson, T. W.; Bailey, S.; Brooun, A.; Bunker, K. D.; Burke, B. J.; Collins, M. R.; Cook, A. S.; Cui, J. J.; Dack, K. N. Design of potent and selective inhibitors to overcome clinical anaplastic lymphoma kinase mutations resistant to crizotinib. *J. Med. Chem.* **2014,** *57*, 1170−1187.

27. Shaw, A. T.; Friboulet, L.; Leshchiner, I.; Gainor, J. F.; Bergqvist, S.; Brooun, A.; Burke, B. J.; Deng, Y.-L.; Liu, W.; Dardaei, L. Resensitization to crizotinib by the lorlatinib ALK resistance mutation L1198F. *N. Engl. J. Med.* **2016,** *374*, 54−61.

28. Shin, S.; Mah, S.; Hong, S.; Park, H. Discovery of low micromolar dual inhibitors for wild type and L1196M mutant of anaplastic lymphoma kinase through the structure-based virtual screening. *J. Chem. Inf. Model.* **2015,** *56*, 802−810.

29. Valente, S.; Liu, Y.; Schnekenburger, M.; Zwergel, C.; Cosconati, S.; Gros, C.; Tardugno, M.; Labella, D.; Florean, C.; Minden, S. Selective non-nucleoside inhibitors of human DNA methyltransferases active in cancer including in cancer stem cells. *J. Med. Chem.* **2014,** *57*, 701−713.

30. Hazeldine, S. T.; Polin, L.; Kushner, J.; White, K.; Corbett, T. H.; Biehl, J.; Horwitz, J. P. Part 3: synthesis and biological evaluation of some analogs of the antitumor agents, 2-{4-[(7-chloro-2-quinoxalinyl) oxy] phenoxy} propionic acid, and 2-{4-[(7-bromo-2-quinolinyl) oxy] phenoxy} propionic acid. *Bioorg. Med. Chem.* **2005,** *13*, 1069−1081.

31. Allen, F. H.; Kennard, O.; Watson, D. G.; Brammer, L.; Orpen, A. G.; Taylor, R. Tables of bond lengths determined by X-ray and neutron diffraction. Part 1. Bond lengths in organic compounds. *J. Chem. Soc., Perkin Trans. 2* **1987**, S1−S19.

32. Johnson, T. W.; Richardson, P. F.; Bailey, S.; Brooun, A.; Burke, B. J.; Collins, M. R.; Cui, J. J.; Deal, J. G.; Deng, Y. L.; Dinh, D.; Engstrom, L. D.; He, M.; Hoffman, J.; Hoffman, R. L.; Huang, Q.; Kania, R. S.; Kath, J. C.; Lam, H.; Lam, J. L.; Le, P. T.; Lingardo, L.; Liu, W.; McTigue, M.; Palmer, C. L.; Sach, N. W.; Smeal, T.; Smith, G. L.; Stewart, A. E.; Timofeevski, S.; Zhu, H.; Zhu, J.; Zou, H. Y.; Edwards, M. P. Discovery of (10*R*)-7-amino-12-fluoro-2,10,16-trimethyl-15-oxo-10,15,16,17-tetrahydro-2*H*-8,4-(metheno)pyrazolo[4,3-*h*][2,5,11]-benzoxadiazacyclotetradecine-3-carbonitrile (PF-06463922), a macrocyclic inhibitor of anaplastic lymphoma kinase (ALK) and c-ros oncogene 1 (ROS1) with preclinical brain exposure and broad-spectrum potency against ALK-resistant mutations. *J. Med. Chem.* **2014**, *57*, 4720−4744.

33. Hatcher, J. M.; Bahcall, M.; Choi, H. G.; Gao, Y.; Sim, T.; George, R.; Jänne, P. A.; Gray, N. S. Discovery of inhibitors that overcome the G1202R anaplastic lymphoma kinase resistance mutation. *J. Med. Chem.* **2015**, *58*, 9296−9308.

34. Kim, H. R.; Kim, W. S.; Choi, Y. J.; Choi, C. H.; Rho, J. K.; Lee, J. C. Epithelial-mesenchymal transition leads to crizotinib resistance in H2228 lung cancer cells with EML4-ALK translocation. *Mol. Oncol.* **2013**, *7*, 1093-1102.

Table of Contents Graphic